Fatigue Flexural Behaviour of Reinforced Concrete Beams with Non-Prestressed and Prestressed Basalt Fiber Reinforced Polymer Bars

by

Taha Younes

A thesis

presented to the University of Waterloo

in fulfilment of the

thesis requirement for the degree of

Master of Applied Science

in

Civil Engineering

Waterloo, Ontario, Canada, 2015

Author's Declaration

I hereby declare that I am the sole author of this thesis. This is a true copy of the thesis, including any required final revisions, as accepted by my examiners.

I understand that my thesis may be made electronically available to the public.

Abstract

Basalt fibers have recently been introduced as a promising alternative to the existing fiber reinforced polymer (FRP) family. The mechanical properties of basalt FRP (BFRP) bars are, generally, better than those of glass FRP (GFRP) bars. However, they are still lower than those of carbon FRP (CFRP) bars. Also BFRP bars have now been developed that have a higher modulus of elasticity than typical GRFP bars. Only a limited amount of research is available on BFRP bars in structural concrete applications and there is no information on the performance of prestressed basalt bars in reinforced concrete elements subjected to fatigue loading.

Most studies that are available deal only with the flexural behaviour of concrete beams reinforced with non- prestressed and prestressed GFRP and CFRP bars under monotonic and fatigue loading. This thesis presents an experimental study of the flexural behaviour of concrete beams reinforced with non-prestressed and prestressed basalt bars under monotonic and fatigue loading and compares these beam fatigue results with the fatigue behaviour of similar machined basalt rebars tested under fatigue loading in air. Sixteen beams with dimensions of (2400× 300×150mm) and thirteen BFRP bare rebars were tested. The parameters that varied were the level of prestress of the bars (0%, 20% and 40% of their static tension capacity) and the fatigue load ranges. The experimental findings showed a difference in the long life fatigue strength between the beams prestressed to 40% 20% and 0% of the bar strength with the beams with the bars prestressed to 40% of the bar strength showing a higher fatigue strength than of those prestressed to 0% and 20%. For 40% and 20 % prestressed beams, there is no benefit in fatigue performance above 20% and 13% of the ultimate capacity of the beams a level at which calculations showed that the remaining prestress did not close cracks at the minimum load in the fatigue load cycle. When compared on the basis of load range versus cycles to failure, the data

for the three beam types fell onto a single curve at load levels where the remaining prestress after fatigue creep relaxation no longer closed the crack at the minimum load.

Keywords: Basalt bars, prestressed concrete, fatigue, flexural, fatigue creep

Acknowledgements

I am sincerely thankful to have had the opportunity and pleasure of working briefly with my past supervisor Professor Khaled Soudki, may his soul rest in peace. His support and dedication was exceptional. He provided significant help in getting admitted to the University of Waterloo, and provided me with considerable guidance to identify my research topic.

I acknowledge the continuing support of my supervisors Professor Adil Al-Mayah and Professor Tim Topper. They have provided their technical expertise and continuous support during my research and after its completion. I hold both of them in the highest regards both personally and professionally.

I would also like to acknowledge the technical assistance of laboratory technicians Richard Morrison, Douglas Hirst, and Rob Sluban.

I would like to acknowledge both Professors Jeffrey West and Jeffrey Casello for giving the time to read my thesis.

Special thanks to Rayed Al-Yousef, Hesham Abduljabbar, Michael Cohen, Mohammed Zawam, Noran Abdel-Wahab, Slamah Krem, Ayman Shihata and Paulina Arczewska for all of their help

Finally, I would like to thank Pultrall Company for providing basalt bars.

Table of Contents

List of Figures

List of Tables

Chapter 1: Introduction

1.1 Introduction

Many reinforced concrete structures are exposed to serious deterioration problems due to the corrosion of the steel rebar inside the concrete. In 2002, the total cost of corrosion in the USA was $276 billion (Thompson, et al. 2007). Therefore, the need for non-corroding materials has become important. Since many reinforced concrete structures are exposed to corrosion and the durability of the structures under a harsh environment is a concern, the use of fiber reinforced polymer (FRP) composites is growing in many construction and infrastructure applications. The problems related to steel rebar (corrosion, weight, etc.) can be avoided by using FRP in this case we will consider basalt fibers (BFRP) as an alternative since BFRP materials are non-metallic, high strength, and non-corroding. In addition, the BFRP is considered safe, non-toxic material and environmentally friendly because of its manufacturing process that involves melting pure raw materials (Brik 2013).

Structural elements can fail under either static or fatigue loading. Fatigue failure is caused by an accumulation of damage over time under fatigue loads. Fatigue behaviour has been recognized as important in the design of structures such as bridges, concrete pavement, marine structures and high speed railway structures that are exposed to fatigue loading during their working life. A significant amount of research is available on the fatigue behaviour of concrete structures reinforced with steel. However, most of the studies of the behaviour of FRP reinforced concrete have dealt with static loading. There is not much information available on the fatigue behaviour of FRP reinforced concrete and of interest here there is so far none on the basalt FRP studied in this thesis. The fatigue behaviour of concrete structures reinforced with FRP is

affected by fiber type, surface conditions prestressing level. Therefore, the aim of the current study is to study the fatigue behaviour of non-prestressed and prestressed concrete beams reinforced with basalt FRP.

1.2 Challenges

Basalt FRP bars provide an alternative to existing FRP materials for prestressed concrete applications. However, the available research is limited to mechanical properties of basalt bars for short term loading. Basalt FRP bars are investigated as reinforcement bars for non-prestressed and prestressed concrete beams in this thesis. Information is needed on their fatigue and creep behaviour under long term and fatigue loading. The challenge in the present research is to evaluate the potential of basalt FRP bars in a prestressed application involving fatigue loading. In addition to fatigue behaviour, creep and deflection behaviour should be analyzed and compared to the Canadian code provisions. Furthermore, it is a challenge to design and implement a new anchorage system for basalt FRP bars required for prestressed concrete applications.

1.3 Research Objective

Corrosion of the steel reinforcement is the most important factor limiting the life expectancy of steel reinforced concrete structures exposed to a corrosive environment. The main goal of this research is to examine non-corroding BFRP material as an alternative for steel reinforcement.

The objectives of this research are

- To study the fatigue behaviour of reinforced concrete with non-prestressed and prestressed BFRP bars under monotonic and fatigue loading.

- To investigate the mechanical properties of BFRP bars under monotonic and fatigue loading.

1.4 Thesis Organization

The thesis consists of six chapters that are organized as follows:

- Chapter 2 presents a comprehensive literature review on FRP materials properties, prestressed concrete under monotonic and fatigue loading, and long term mechanical properties of FRP.
- Chapter 3 explains the experimental program procedures including the test setup as well as material properties, and the beam's configuration
- Chapter 4 presents an analysis of the load deflection of monotonic tests for basalt bar specimens and compares the test results to the predictions.
- Chapter 5 presents fatigue and fatigue creep results for basalt bar specimens, an analysis of the load strain behaviour of the basalt reinforced beams including fatigue creep strains and predicts the fatigue test results for the basalt bar reinforced beams.
- Chapter 6 presents fatigue test results for the basalt beams and compares them to predictions.
- Chapter 7 reports the main conclusions drawn from the experimental investigation.

Chapter 2: Literature Review

2.1 Fiber Reinforced Polymer (FRP)

Fiber reinforced polymer (FRP) reinforcements, with their outstanding mechanical and non-corroding characteristics have been increasingly accepted as a main flexural reinforcement in concrete structures. FRP composites consist of aligned continuous fibers embedded in a resin matrix. Fibers commonly used are Carbon, Aramid, or Glass, and the corresponding composites are known as CFRP, AFRP, or GFRP, respectively. Commonly used resins are epoxy, polyester, and vinyl ester. Depending on the fiber quality, orientation, length, shape, volumetric ratio, adhesion to matrix, and the manufacturing process, the mechanical performance of a composite will vary.

Unlike steel elastic-plastic behaviour, FRPs exhibit linear stress-strain relationships up to failure, as shown in Figure 2-1. FRP bars normally have a tensile strength higher than that of conventional steel reinforcing bars. This relatively high tensile strength makes FRP bars particularly attractive for prestressed concrete applications. The modulus of elasticity of FRP bars is lower than that of steel bars. In fact, the modulus of elasticity for commercially available GFRP and AFRP bars ranges from 20 to 25 % that of steel (Mohamed 2013), while that of CFRP bars ranges from 60 to 75 % of that of steel (Rafi and Nadjai 2008).

Basalt fiber reinforced polymer (BFRP) composites with an elastic modulus between 50-57 GPa are a recent addition to the family of fiber reinforced polymer composites such as GFRP and CFRP composites used in reinforcing concrete members**.** Compared to GFRP which has a similar cost, BFRP has a higher strength, a higher modulus of elasticity and a better resistance to chemical attack (Van de Velde et al. 2003). It also has a high thermal stability and sound insulating properties and electrical insulating properties that are 10 times better than glass and

can be used in a wider temperature range (-260 °C) to approximately (800 °C) compared to E-glass (-60 to 450-460 °C) (Van de Velde et al. 2003). Although, CFRP has a 2.8 times higher modulus of elasticity and 1.3 times higher ultimate tensile strength than BFRP, BFRP is half cost of CFRP on an equivalent strength basis and same cost on an equivalent stiffness basis.

Since concrete structures such as marine structures, parking garages and bridges are subjected to fatigue loading during their lives, it is important to understand their creep and fatigue behaviour. In addition, the limit states (ultimate and serviceability) governed by fatigue behaviour must be taken into account by designers (Demers 1998a).

There are many factors that affect the fatigue life of reinforced concrete, such as the material properties of the reinforcement and the concrete, the stress range, and the rate of loading (Chang and Kesler 1958). The stress range and the mean stress are considered to be the main loading parameters that affect the fatigue life of structures (Pook Les 2007). Generally, as the stress range and the mean stress increase, the fatigued strength decreases (Pook Les 2007).

At the location of cracks in a concrete structure, FRP tendons bonded to concrete experience high stresses resulting in tendons rupture (Burgoyne 1993). However, unbonded tendons experience a constant stress along the free length between the anchorages, the tendon at a crack location will not develop high local stresses. Therefore, the maximum stress increases at a much slower rate for unbonded rebars than for bonded rebars after concrete cracking, and hence the stress for unbonded bars is usually less than the rupture stress when the beam reaches its ultimate capacity. It can be concluded that lack of bonding avoids a sudden failure of FRP tendons and increases the ductility of the unbonded concrete structure since the stress increases at higher rate in bonded tendons than for unbonded tendons (Mutsuyoshi et al. 1990; Alkhairi 1991; Kato and Hayashida 1993).

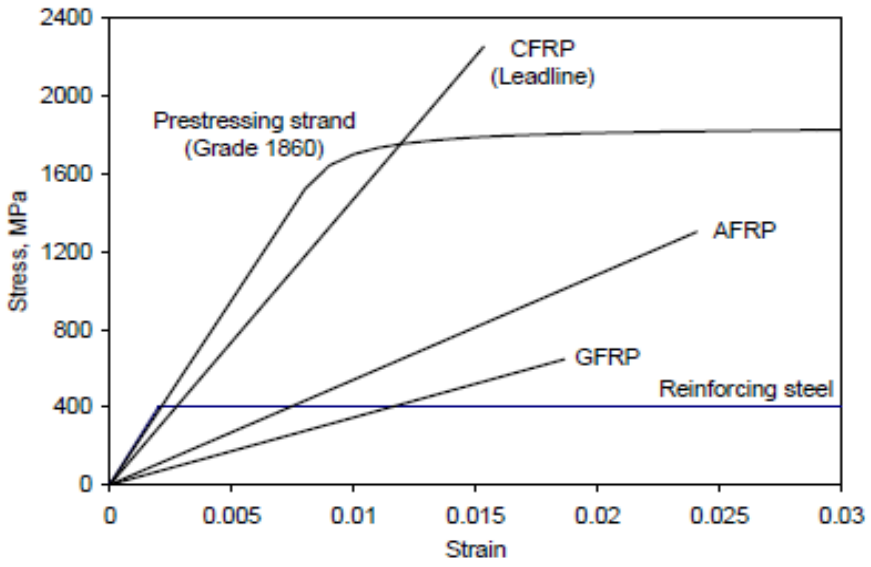

Figure 2- 1 *Stress-strain relationship of different rebars materials (ISIS Canada 2008)*

2.2 Long Term Mechanical Properties of FRP

The long term mechanical properties of FRP differ significantly from those of steel in terms of creep and fatigue behaviour as explained in the upcoming sections. Therefore, it is essential to understand the mechanical behaviour of FRP composites and take them into account in the design process.

2.2.1 Creep

Creep is defined as the deformation of a material with time under a constant load. The main issue that needs to be addressed related to creep of FRP in design is the increase in creep strain under long term static and fatigue loading (Balazs and Bronosyoi 2001).

Generally, FRP materials show an initial elastic strain when a load is imposed. After this elastic deformation if the load is high enough there is a primary stage of creep in which the slope of the strain versus time curve decreases as the strain increases. Then there is a second stage of steady- state creep, which is distinguished by a constant strain rate under a constant stress which

continues for a period of time. In this stage, the weaker fibers may fail. However, the resin between the fibers transfers the stress to adjacent fibers (ACI 440 2006). In a tertiary stage, which can occur at a high stress, the strain then accelerates rapidly up to failure. At lower stresses, the secondary creep rate may decrease until creep ceases altogether.

Figure 2- 2 shows a typical creep strain curve of AFRP bars, which follows three stages: primary, secondary and final stage in which failure occurs (ACI 440 2006). However, for CFRP bars the strain rate during the second stage falls to zero as shown in Figure 2- 3.

Glass and carbon fibers have a good resistance to creep; on the other hand, polymeric resins are more susceptible to creep; as a result, fiber type, volume fraction and fiber orientation and temperatures which lead to a decrease in resin strength play an important role in the creep performance of FRP reinforcing rebar (FIB 2007).

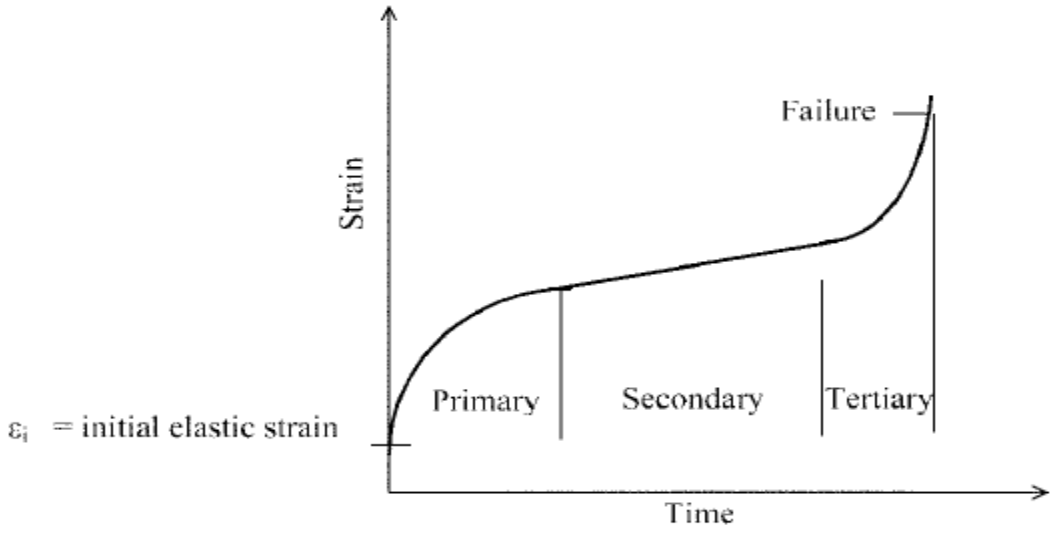

Figure 2- 2 *A typical creep strain curve of AFRP bars (ACI 440 2006)*

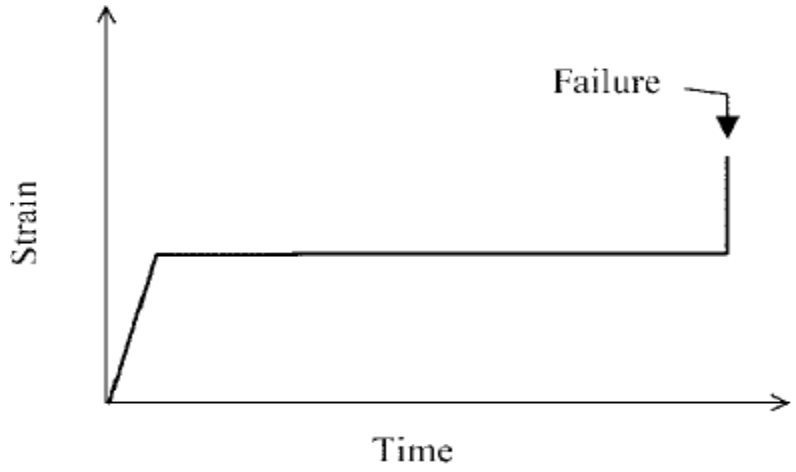

Figure 2- 3 *A typical creep strain curve of Carbon bars (ACI 440 2006)*

2.2.2 Behaviour of FRP under Fatigue Loading

ACI 440 (2006) indicates that the mean stress and the ratio of maximum and minimum stress are factors that affect the endurance limit of CFRP bars. Since the stiffness of GFRP is lower than CFRP material, GFRP is more influenced by fatigue loading (Curtis 1989, 1991). The Log - Log S-N curve for GFRP, generally, has a steeper slope than that for CFRP materials which exhibit an almost flat trend line (Konur and Matthews 1989).

The failure of homogenous metals due to fatigue loading generally occurs in a single mode by the initiation and propagation of a crack until final failure. However, FRP material exhibits different modes of failure, which include matrix cracking, fiber-matrix debonding, void growth and finally fiber rupture (El-Ragaby et al. 2007, Kim and Ebert 1978). Fatigue failures of composite material are attributed to damage accumulation rather than the propagation of a single crack (Reifsnider 1991).

It has been observed that the predominant variable causing fatigue failure is the range of the applied stress or strain. It has been suggested that the FRP fatigue life curve is defined by three different damage mechanisms as shown in Figure 2- 4 (Talreja 1981a, Brondsted et al.

1997), each operating in a different range of strain levels. At the highest strains, the failure is attributed to fiber breakage and interfacial debonding. As the number of broken fibers increases, the stress in the remaining fibers progressively increases and they break with increasing frequency until failure takes place. In the second region failure is dominated by matrix cracking and interfacial shear. Finally at low stress levels, no propagating cracks are initiated leading to an endurance limit below which no failures occur.

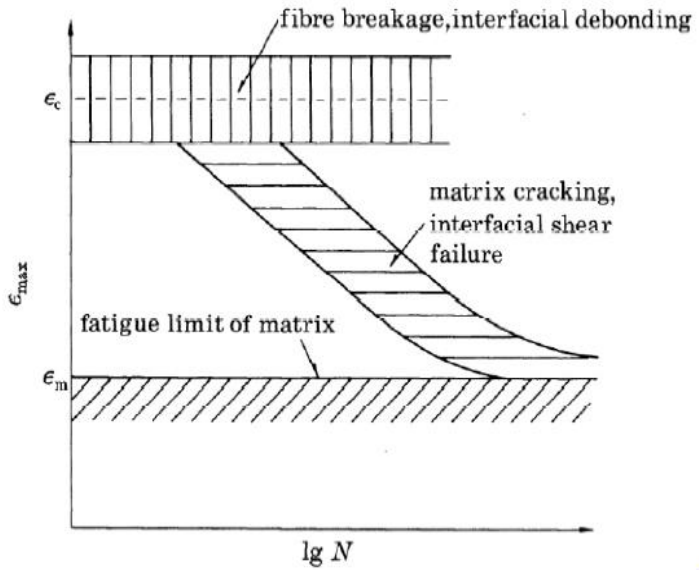

Figure 2- 4 *Fatigue life diagram for unidirectional composites (Talreja 1981a)*

It has been reported that FRP has a good fatigue performance compared to steel in the form of bare bars (Saadatmanesh and Tannous 1999, El-Ragaby et al. 2007a, Braimah 2000). Preliminary fatigue test results carried out by (El Refai 2013) showed that the fatigue limit of BFRP bars was about 4% of their ultimate capacity. However, the fatigue limit of GFRP bars was about 3% of their ultimate capacity. Furthermore, the results showed that BFRP has a low sensitivity to water moisture and is a durable material. Therefore, it was suggested that it would be suitable for use as prestressing or non-prestressing reinforcement. A study conducted by

Dorigato and Pegoretti (2012) to investigate the behaviour of BFRP laminates under fatigue load showed better fatigue performance than glass fiber laminates.

2.3 Behaviour of Concrete under Fatigue Loading

Concrete stress-strain behaviour is also influenced by fatigue loading. The fatigue of concrete appears clearly as an inelastic strain in the form of cracks and creep (Heffernan and Erki 2004). The effect of creep on the fatigue life of concrete becomes clearer at high stress ranges (Award and Hilsdorf 1974). The initiation and propagation of cracks are caused by the collapse of the bond between the aggregate and matrix (Murdock and Kessler 1960). In plain concrete Antrim (1967) concluded that fatigue failure is attributed to the growth of micro cracks that formed in the cement paste, which leads to the deterioration of the concrete until failure occurs. Holmen (1982) concluded that the micro-cracks are the main initiating sites of the cracks that cause the fatigue failure of concrete. The frequency of loading has little effect on concrete fatigue behaviour if the maximum stress held to 75% of the static strength (Rezansoff et al. 1993). An endurance limit was not observed for concrete subjected to less than 10 million cycles (Rezansoff et al. 1993).

ACI 215 (1997) established a rough estimate that at 10 million cycles, the fatigue strength of concrete is about 50-55% of its static strength for compression, tension or flexure. Whether the plain concrete is loaded in tension, compression or flexure, the fatigue strength in terms of the corresponding static strength is similar (ACI 215 1997) as shown in Figure 2- 5. The findings by Thun et al. (2007) from cyclic uniaxial tensile tests on plain cylindrical concrete cores showed that the fatigue limit cannot be predicted exactly. However, for cycling with a mean load level of 40% of the ultimate tensile strength and an amplitude of 40% of the tensile strength, a low deformation rate and a limit to fatigue failures were obtained.

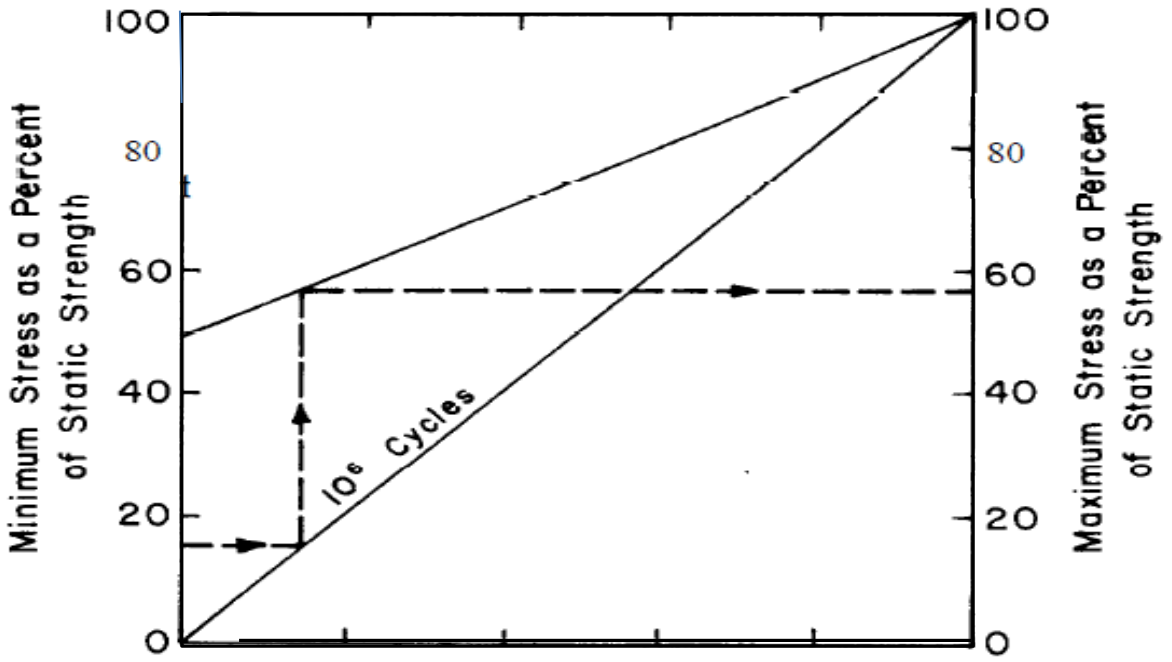

Figure 2- 5 *Fatigue strength of plain concrete in tension, compression and flexure (ACI 215R-74 1997)*

The application of fracture mechanics of concrete differs from its application to ductile materials which exhibit yielding at the tip of a fatigue crack. Concrete is a brittle material that does not exhibit traditional plastic behaviour in tension. However, micro-cracks occur before fracture (Bazant 1985). These microcracks create a strain softening region at the tip of a fatigue crack. The majority of this nonlinear zone will exhibit strain softening rather than the strain hardening typical of a ductile material (Bazant 1985).

Glucklich (1965) studied the initiation of the cracks in mortar beams. He concluded that the cracks can be initiated or propagated if the structure is subjected to a high stress applied once or a lower stress fatigue many times. Mindess and Young (1981) concluded that during the hydration process, high stresses are generated at the cement matrix and aggregate interface due

to shrinkage. Once these stresses exceed the strength of the cement- aggregate bond, cracks can be propagated under fatigue load even if the nominal stresses in concrete are low.

2.4 Prestressed FRP Reinforced Concrete Members

FRP materials generally have good fatigue properties and exhibit low relaxation losses, both of which are important to the service lives and load-carrying capacities of reinforced and prestressed concrete structures (ISIS Canada 2008). It has also been reported that FRP has a good fatigue performance compared to steel in the form of bare bars (Saadatmanesh and Tannous 1999, El-Ragaby et al. 2007a, Braimah 2000). As a reinforced concrete beam is loaded monotonically, the strain resulting from the applied load increases. When the concrete tensile stress at the bottom of a beam due to the imposed load reaches the concrete cracking stress, the concrete cracks and the load-strain curve of the reinforcing bar shows an abrupt increase in strain as the strain increases until the reinforcement has taken up the tensile force shed by the cracked concrete as shown in Figure 2- 6. Afterwards, the load -strain curve continues at a higher slope since the applied load is carried only by the rebar. However, during unloading following cracking the load strain curve will follow the dashed line of Figure 2- 6 since the cracked concrete will no longer contribute to the tensile force. On subsequent load cycles the load strain curve will continue to follow the dashed line.

A similar behaviour is seen for a prestressed beam in Figure 2- 7. Again, there is an abrupt increase in the strain in the load-strain curve of the reinforcing bar as the concrete at the bottom of the beam cracks followed by an increase in slope as further tensile forces are taken by the reinforcement. On unloading, the load-strain follows the dashed curve until the crack closes due to the prestressing force. Then it follows the original loading curve as force changes are shared by the reinforcement and the concrete.

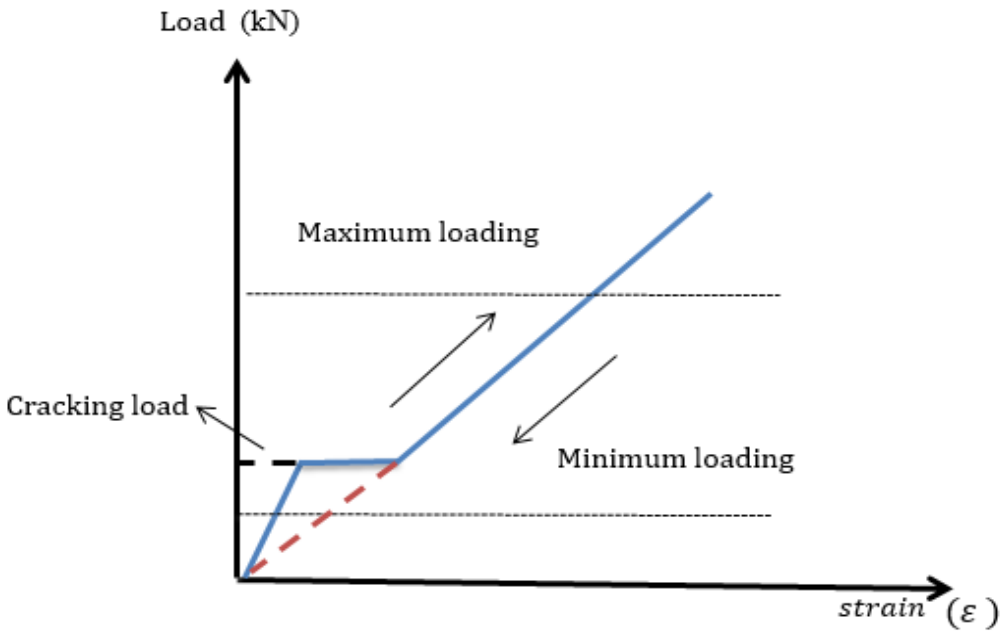

Figure 2- 6 *Load- strain relationship of non- prestressed concrete under fatigue*

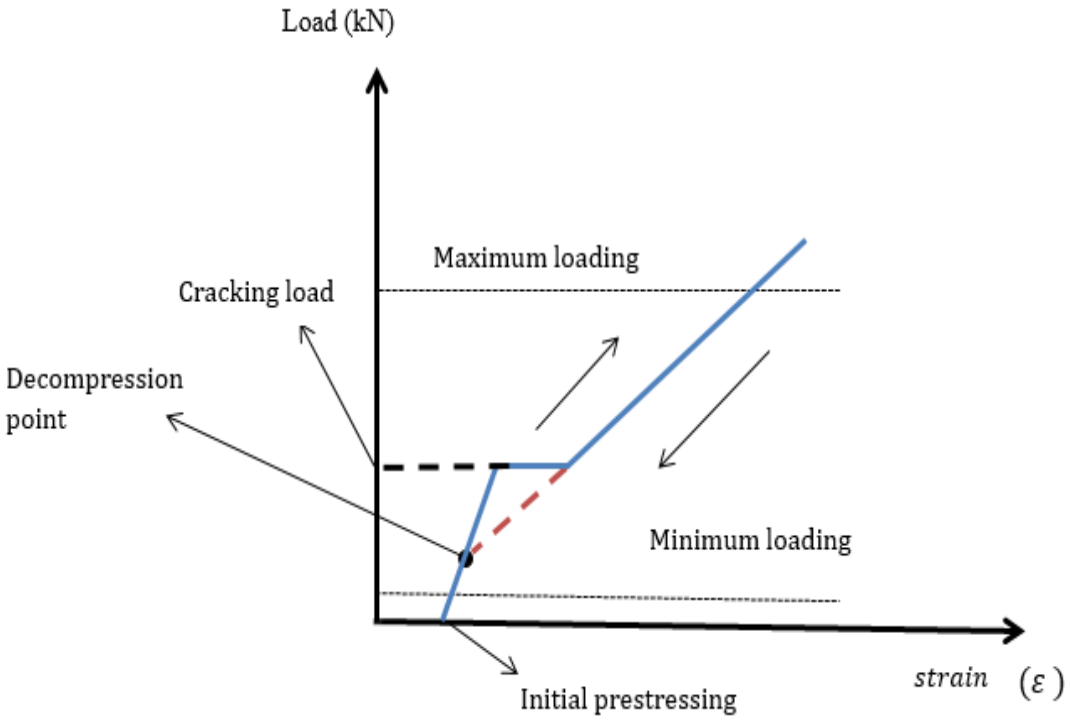

Figure 2- 7 *Load- strain relationship of prestressed beams under fatigue* loading

Finally, most of the studies that have been conducted dealt with the behaviour of carbon and glass fibers tested under monotonic and fatigue loads. From the author's perspective there is no previous published data found on the flexure behaviour of concrete beams reinforced with non-prestressed and prestressed basalt rebars under fatigue load. Therefore, the current study aims to investigate the flexural behaviour of non-prestressed and prestressed basalt bars in beams under fatigue loading and compare the data with fatigue results for the bare basalt bars tested in air.

Chapter 3: Experimental Program

3.1 Introduction

This chapter presents the experimental program of the current study. The experimental program consists of tests of thirteen machined basalt bars and sixteen non-prestressed and prestressed concrete beams reinforced with basalt bars. The basalt bars and concrete specimens were tested to evaluate their fatigue lives under cycling loading. Also, it presents the instrumentation and material properties for both basalt bars and concrete.

3.2 Machined Bare Basalt Bars

The thirteen bare basalt bars were tested in this study until failure, three of which were tested monotonically in displacement control and one bar tested under sustained load. However, the other nine basalt bars were tested in load control under fatigue load at different stress range. The aim was to compare the fatigue lives of the bare basalt bars to those of identical basalt bars at identical stress levels in the prestressed concrete beams.

The basalt bars in the current study were sand- coated with a diameter of 12.45mm. The bar fatigue specimens were 630 mm in length, and all of the bars were tested to failure under fatigue loading. All of the specimens were gripped using same anchorage that was developed at the University of Waterloo (Al-Mayah el at. 2006) as shown in Figure 3- 1. At the beginning, some preliminary axial fatigue tests were carried out on the as-received BFRP bars. In these tests there was a premature failure at the anchors due to local stress concentrations at the end of the steel wedges. Subsequently, the BFRP rebars were machined to reduce the diameter of the bar to 6.225 mm at the middle of the bar as shown in Figure 3- 2. The longitudinal radius of the

reduced section was 1225 mm resulting in a very small stress concentration and all failures occurred in the reduced section rather than at the grips.

Figure 3- 1 *Anchorage components used for prestressing*

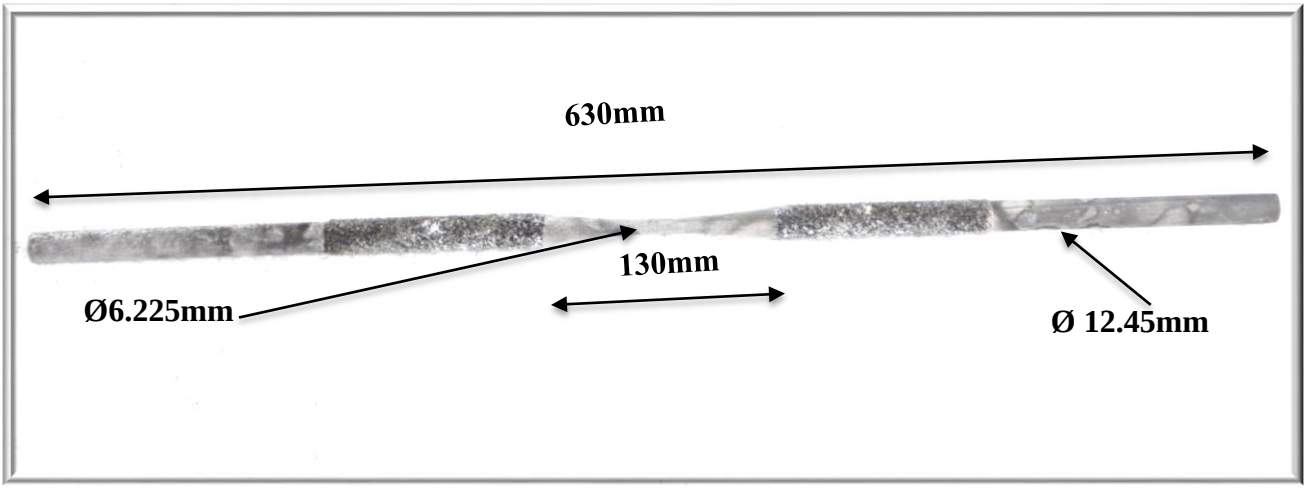

Figure 3- 2 *BFRP axial fatigue test specimens*

3.2.1 Instrumentation and Testing of Machined Bare Basalt Bar Fatigue Specimens

At the beginning of a test, the bar fatigue specimen was loaded up to the maximum load and then unloaded to the mean load in order to seat the wedges in the anchor. The minimum load was kept constant for all the specimens. The minimum stress can be calculated using Equation (1). This equation was used to calculate the minimum stress in the fatigue tests of prestressed beams since at this load level the cracks were closed as a result of the prestress.

$$f = \left(\frac{M * Y_e}{I_g}\right) * n + f_{pe} \qquad \text{..... (1)}$$

Where: f = minimum stress in BFRP bar.

M = applied moment.

Y_e = distance from elastic centroid of transformed section to location of BFRP bar.

I_g = gross transformed section moment of inertia

f_{pe} = effective prestress after losses, including elastic shortening.

n = modulus ratio = $\frac{E_{frp}}{E_c}$

The maximum stress that was experienced by the embedded bars under fatigue loading was calculated using a prestressed-cracked section analysis since for all peak stress levels the cracks were open. The specimens were tested at a frequency of 6 Hz. Two strain gauges were mounted in the critical section in order to measure the fatigue strains. The specimens that reached one million cycles (a run out limit) were retested at a higher load range. Since 1,000,000 cycles could be reached in a reasonable amount of time, it is considered as a run out limit. All of the specimens were tested in the test frame with a hydraulic actuator shown in Figure 3- 3. Since

it is a new material to be tested under fatigue loading, its fatigue life cannot be predicted. The stress range for the first tested bar was chosen to be 50% of the ultimate basalt bar capacity a level that was expected to result in a finite fatigue life. Table 3- 1 gives test matrix for the tested machined bars.

The machined basalt bar was also tested under a sustained load of 50% of the ultimate capacity of the basalt bar to determine whether static creep was important in the fatigue tests. Two strain gauges were fixed at the critical section in order to measure the creep strain.

Table 3- 1*Test matrix of the machined bars*

Notation*	Loading Type	Minimum Loading (kN)	Maximum Loading (kN)	Expected Fatigue life
	Monotonic	---------	36	------
FBB-1	Fatigue		35	N/A
FBB-2	Fatigue		32	N/A
FBB-3	Fatigue		30.25	N/A
FBB-4	Fatigue		28.5	N/A
FBB-5	Fatigue	14.5	24	N/A
FBB-6	Fatigue		22.9	N/A
FBB-7	Fatigue		21.4	N/A
FBB-8	Fatigue		19.9	N/A
FBB-9	Fatigue		17.2	N/A

FBB: Stands for fatigue bare bar and last number refers to the number of the specimen

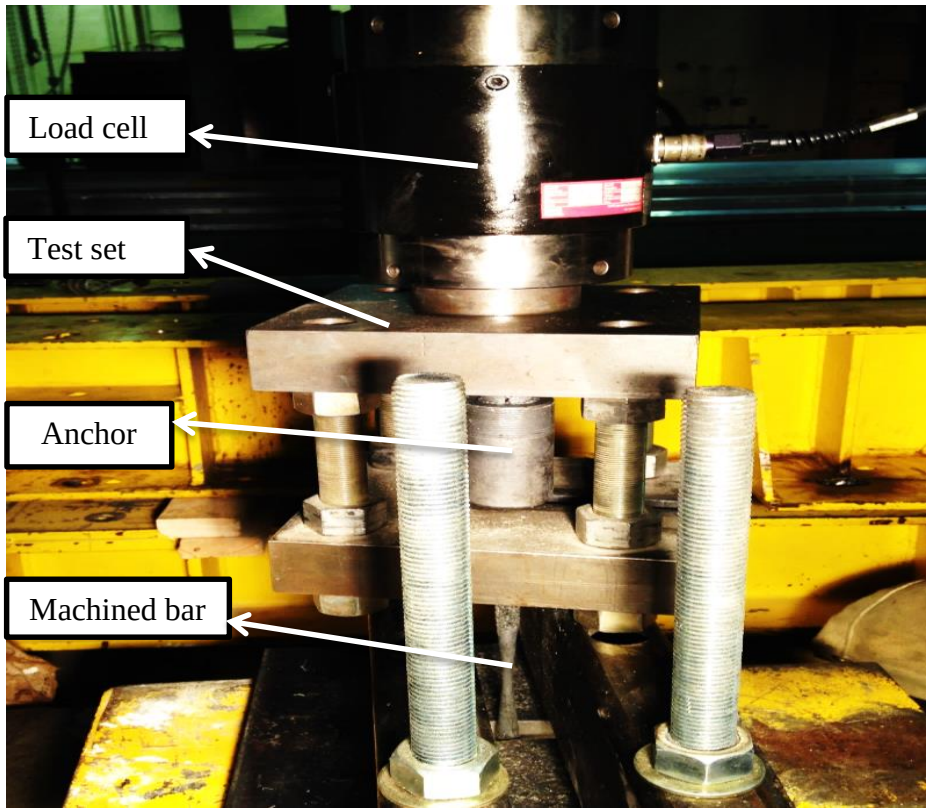

Figure 3- 3 *Bar in test frame with wedge anchors*

3.2.2 Properties of the Bare Basalt Bars

The rebar has a sand coated surface. The mechanical properties of the BFRP rebars, were determined from a tensile test conducted at the University of Waterloo. Table 3- 2 gives the mechanical properties of the tested bars.

Table 3- 2 *Mechanical properties of the tested bars*

Specification	Sand coated Bars
Actual diameter (mm)	12.45
Reduced diameter (mm)	6.225
Ultimate tensile capacity for the non- machined bar (MPa)	1456
Ultimate tensile capacity for the machined bar (MPa)	1183
Modulus of elasticity (GPa)	53.3
Actual area(without machining)(mm^2)	121.7
Area of the critical section(reduced part)	30.41

3.3 Concrete Beams

Sixteen non-prestressed and prestressed concrete beams reinforced with basalt bars were investigated. The beams were divided into three groups. The first group had six non- prestressed beams. The second group had six beams that were prestressed to a bar stress of 40% of the material's static tension capacity and the third group had four beams that were prestressed to a bar stress of 20% of the materials tension capacity. Two beams, one from the first group and the other one from the second group were monotonically loaded to failure under deflection control at a rate of 1 mm per minute and served as a controls for all groups, because the expected ultimate load capacity for the third group under monotonic loading is the same as the other two groups. The expected mode of failure for both prestressed and non prestressed beams was by the bar rupture. In order to study the effect of prestressing level (0%, 20% and 40% of the bar failure load) on the fatigue life of BFRP reinforced beams, five beams of the first group, five beams

from the second group, and four beams of the third group were subjected to fatigue loads under load-control. Table 3- 3 gives a test matrix of the tested beams.

The minimum load in the load cycle for the fatigue beam specimens was kept equal to 10% of the 85 kN ultimate strength of the control beam. The fatigue life for all the tested beams was predicted based on the results obtained from the fatigue life of the bars that were tested in air. One beam from groups two and three was tested again at a higher load range after it had reached the run out limit (1,000,000 cycles).

Table 3- 3 *Matrix of tested beams*

Group	Description	Loading Type	Minimum Loading (%)	Maximum Loading (%)	Load Range (%)
One	Non-Prestressed Beams	Monotonic	---------	---------	---------
		Fatigue	10	55	45
		Fatigue	10	35	25
		Fatigue	10	28	18
		Fatigue	10	24	14
		Fatigue	10	21.5	11.5
Two	40% Prestressed Beams	Monotonic	--------	---------	---------
		Fatigue	10	90	80
		Fatigue	10	70	60
		Fatigue	10	58	48
		Fatigue	10	45	35
		Fatigue	10	37	27
		Fatigue	10	30	20
Three	20% Prestressed Beams	Fatigue	10	80	70
		Fatigue	10	65	55
		Fatigue	10	36	26
		Fatigue	10	28	18
		Fatigue	10	23	13

3.3.1 Description of Concrete Beams

The concrete beam dimensions were 2400 mm in length 300 mm in height and 150 mm in width as shown in Figure 3- 4. Six beams were non-prestressed and ten beams were pretensioned (six prestressed to 40% and four to prestressed 20%). All of the beams were simply supported over a length of 2200 mm center to center and subjected to two equal central loads, spaced 300 mm apart, to produce a constant moment region in the middle of the beam. The expected mode of failure for all the tested beams is a tension failure of the basalt reinforcing bar. This configuration creates two equal shear regions with lengths of 950 mm each. The configuration was designed to avoid bond failure and ensure flexural failure. All of the beams were reinforced with one basalt bar in the tension region with a diameter of 12.45mm. Two 10M Grade 400 deformed steel bars were provided in the compression zone. The clear concrete cover of 35 mm was kept constant for all the beams. In order to avoid shear failure and assure that a flexural failure occurred, adequate shear reinforcement was provided, in the form of 10 M stirrups spaced at 100 mm center to center.

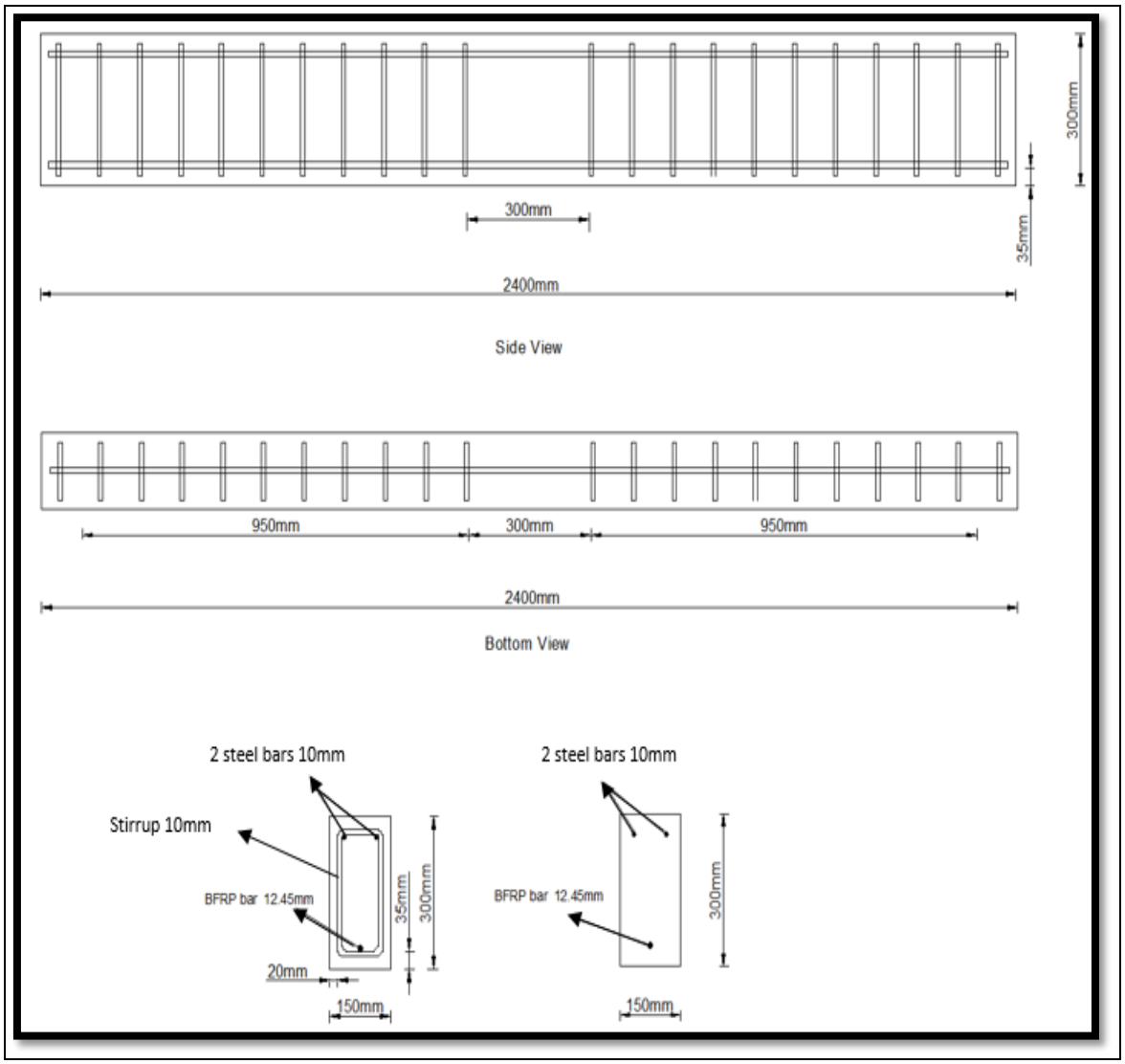

Figure 3- 4 *Typical beam specimen*

3.3.2 Instrumentation and Testing of Concrete Specimens

Sixteen steel cages and formwork were prepared as shown in Figure 3- 5. The control beam was loaded monotonically to failure; the load was applied by a hydraulic jack through a load cell, and a steel spreader beam that transferred the load to the test beam. All the beams were loaded in four- point bending as shown in Figure 3- 6. Nine strain gages were used in one of the prestressed beams (40% prestressing), which was tested under monotonic loading. The gages were fixed on the tension reinforcement, three of which were in the constant moment region and

three in each of the two shear spans at distances of 100 mm, 250 mm, and 500 mm from the support to measure the strain in the tension reinforcement during prestressing and flexural loading. For the other nine beams a total of three strain gauges were placed in the moment constant region only, two of which were placed under the point loads on each side and one was mounted in the middle of the moment constant region. In order to fix the strain gauges, the sand coating of the rebar was removed and the surface of rebar was flattened and cleaned. Then the strain gauges were coated with wax in order to protect them from any damage during casting.

In addition, two concrete strain gauges were mounted on the concrete, one at the top of the concrete at the centre of the moment constant region and the other one in the middle of the concrete compression region at the centre line of the beam. A linear variable differential transducer (LVDT) was placed at the mid span of the beam to measure the deflection.

Ten basalt rebars were prestressed. Six of them were prestressed to 40% of their ultimate capacity and four basalt rebars were prestressed to 20% of their ultimate capacity. Anchorage components used for prestressing are shown in Figure 3- 1.

To eliminate a stress concentration that can lead to premature failure in the anchor zone, at the interface between the grip and the prestressed bars, the BFRP bars were stressed using a prestressing system having an anchor designed to eliminate this problem developed at the University of Waterloo (Al-Mayah el at. 2006). The surface at the end of each BFRP bar was cleaned using acetone before anchoring. In order to distribute the stress on the surface of the bar and prevent the wedges from notching the bar, copper sleeves were placed on the bar and then three steel wedges were pushed firmly into the barrel of the grip after they had been assembled around the sleeve. To reduce the friction between the barrel and the wedges, the outer surface of the steel wedges was lubricated with G-n Metal Assembly Paste, and then the wedges were

seated into the barrel that was fitted into a steel plate using a hydraulic jack as shown in Figure 3- 7.

Figure 3- 5 *Form work used to cast all the beam specimens*

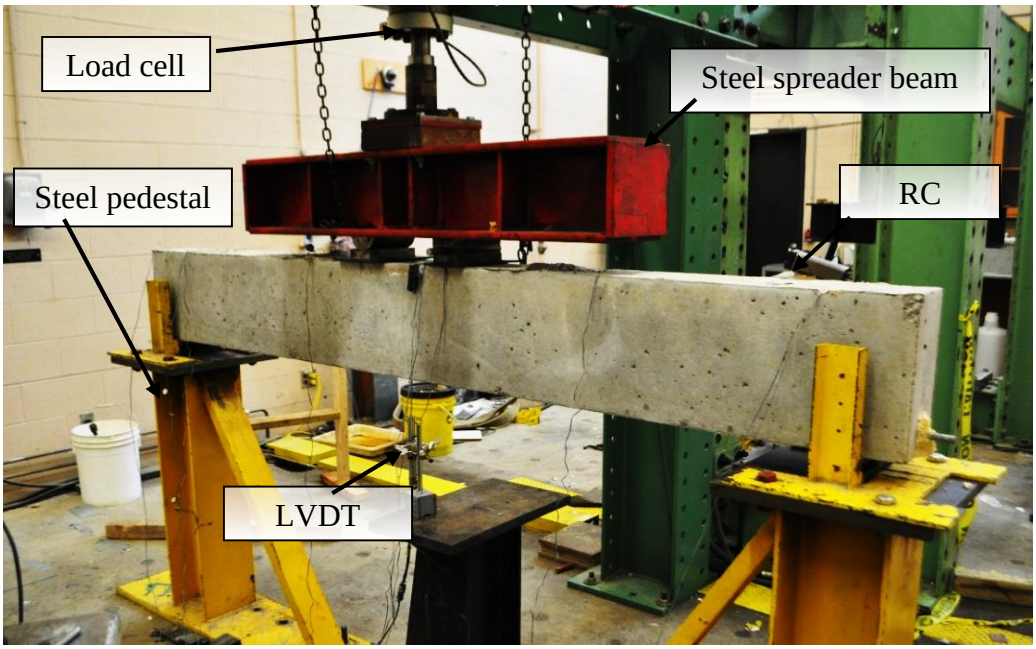

Figure 3- 6 *Beams Test set up*

Figure 3- 7 *Hydraulic manual pump and jack used in pre-seating the anchor*

3.3.3 Properties of Concrete

The tested beams were cast from two batches of concrete. All of the prestressed beams, 40% and 20% were cast from one batch; however, the non- prestressed beams were cast from another batch. The concrete used for the beams was designed to achieve a target compressive strength of (55 MPa) after 28 days. For each of the sixteen beams, cylinders with dimensions of 100mm in diameter and 200 mm in height were cast and tested to determine the compressive strength of the concrete. Five cylinders were tested at the time of releasing the prestressed bars, and another five were tested 28 days after the pouring of the beams. For prestressed beams, the average of compressive strength after 28-days for five cylinders of the concrete was 50 MPa. For the non-prestressed beams, the average after 28 was found to be 55 MPa.

Chapter 4: Monotonic Loading Beams Test Results

4.1 Introduction

This chapter presents the behaviour and the results of the two beams that were tested monotonically to failure. One beam was non- prestressed and the other was prestressed to 40% of the ultimate capacity of the rebar. The load deflection behaviour, the mode of failure, the cracking load and the ultimate load of the two beams are discussed.

4.2 Prediction of Deflection

After cracking, the stiffness of a concrete member is reduced. The reduced stiffness of the member can be taken into account in deflection calculations by using an effective moment of inertia of the cracked section or a bilinear moment curvature diagram (CSA 2004). ACI 440.4R (2004) suggests the use of a linear elastic analysis to calculate deflections of concrete beams by introducing an effective moment of inertia, I_e, as given in Equation (2) for prestressed beams and as given by Equation (3) for non-prestressed beams. For equal concentrated symmetrically placed loads, maximum deflection at the center of the span is given by Equation (4). However, experimental results have shown that Equations (2) and (3) are not reliable for FRP reinforced concrete members (Razaqpur et al. 2000). Therefore, it has been suggested that a moment-curvature relation for FRP reinforced concrete sections using a stress block diagram, Equations (5) and (6), should be used in order to estimate the deflection accurately (Razaqpur et al. 2000).

I_e For a prestressed beam is given by:

$$I_e = \left(\frac{M_{cr}}{M_a}\right)^3 * I_g * \beta + \left(1 - \left(\frac{M_{cr}}{M_a}\right)^3\right) * I_{cr} \leq I_g \quad \ldots\ldots\ldots\ldots\ldots\ldots\ldots\ldots\ldots (2)$$

Where: $M_{cr} = (0.6*\sqrt{f_c} + \frac{P}{A_g} + \frac{P*e*y}{I}) * \frac{I_g}{Y_b}$,

I_{cr} = moment of inertia of cracked section,

M_a = maximum moment due to the specified loads,

A_g = gross area of the beam cross-section,

e = eccentricity of an internal prestressing tendon,

P = effective value of the prestress force,

y_b = distance from the extreme bottom fiber to the centroid of the gross section,

$\beta = 0.5\left\lfloor\frac{E_P}{E_s} + 1\right\rfloor$

I_g = gross section moment of inertia

Where: E_P is modulus of elasticity for FRP, and E_s is modulus elasticity for steel.

I_e For a non-prestressed beam is given by:

$$I_e = \left(\frac{M_{cr}}{M_a}\right)^3 * I_g + \left(1 - \left(\frac{M_{cr}}{M_a}\right)^3\right) * I_{cr} \leq I_g \quad \ldots\ldots\ldots\ldots (3)$$

Where: $M_{cr} = \frac{f_r * I_{tr}}{y_{cr}}$

f_r = modulus of rupture,

M_{cr} = cracking moment,

M_a = maximum applied moment,

I_g = gross section moment of inertia,

I_{cr} = moment of inertia of a cracked section,

I_{tr} = moment of inertia of transformed section,

The maximum deflection at the center of the span is given by

Δ max (at center) $= \frac{P\,a}{24\,E_c\,I_e}(\,3\,L^2 - \,4\,a^2\,)$ ... ... (4)

Where:

P = (Total applied load / 2)

a = shear span

L = length of the beam from support to support.

I_e = effective moment of inertia

E_c = modulus of elasticity of the beam

Using Moment-Curvature Relation of FRP Reinforced Concrete Section to calculate I_e:-

The curvature is given by

$$\emptyset = \frac{\varepsilon_c}{c} = \frac{\varepsilon_F}{(d\,-\,c)} \qquad \text{..... (5)}$$

Where:

ε_c = the concrete strain in the extreme fiber in compression

c = the depth of the neutral axis

d = the effective depth of the beam

ε_F = the strain in the FRP layer located at a distance *d* from the extreme fiber in compression.

ε_F and ε_c are caculated based on strain compatiblity at a given load level.

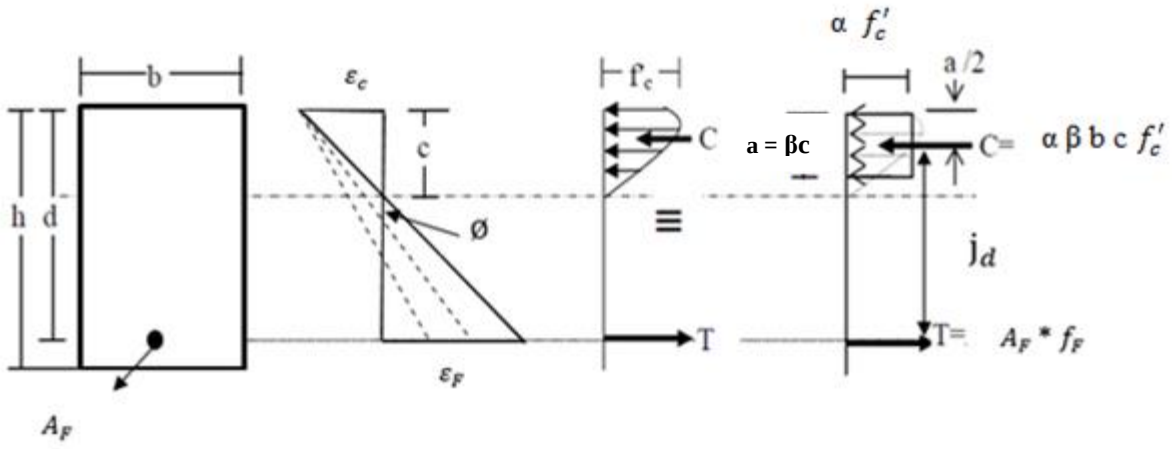

Figure 4- 1 *Stress stain profile*

Procdure for the caculation of I_e by using the stress block diagram

1- Assume various values for ε_c in order to determine the corresponding *c* values by using the equilibrium of forces acting on the section (C = *T)* as shown in Figure 4- 1.

Where

(C) is the resultant compressive force acting on the uncracked concrete.

C = α*β*f'_c *c *b …… (7)

Where

$\alpha * \beta = \frac{\epsilon_t}{\epsilon'_c} - \frac{1}{3} * (\frac{\epsilon_t}{\epsilon'_c})^2$

$\beta = \frac{4 - \frac{\epsilon_t}{\epsilon'_c}}{6 - 2* \frac{\epsilon_t}{\epsilon'_c}}$

Where

ϵ_t is the extreme fiber compressive strain, and ϵ'_c is the strain when f_c reaches f'_c

$\epsilon'_c = \frac{f'_c}{E_c} * \frac{n}{n-1}$, where n = 0.8 + $\frac{f'_c}{17}$ MPa, and E_c is the modulus of concrete

(T) is the net tension in the reinforcement

T =$A_F * f_F$ ……. (8)

Where A_F the cross section area of BFRP, and f_F is the stress in BFRP and can be calculated as following:

f_F = $E_F \times \varepsilon_F$ ……. (9)

Where

E_F is the modulus of elasticity of BFRP, and ε_F is the strain in BFRP. The strain in BFRP can be calculated as following:

$\varepsilon_F = \varepsilon_c \times \left(\frac{d}{c}\right) + \varepsilon_{pe} - \varepsilon_c$ …….. (10)

Where ε_{pe} is the effective strain in FRP due to stressing.

2- Calculate the moment corresponding to the assumed strain profile using (M = $T\ j_d$), where j_d is the internal moment lever arm

3- Cacaulate I_e by using

$I_e = \frac{M_s}{E_c * \emptyset} < I_g$ …….(11)

Where

M_s= moment at a given load level

E_c = modulus of elasticity of concrete

4- The obtained value of (I_e) from (Eq.11) should be used in (Eq.4) to calculate the deflection at midspan.

4.2.1 Deflection at Ultimate Load

In the current study, the beam deflection at the mid span was predicted by calculating Ie by the proposed equation (2) for prestressed beams, and Equation (3) for non-prestressed beams. The moment curvature approach was also used to calculate (I_e). After (I_e) was calculated, Equation (4) was used to calculate the deflection at the center of the span.

For the 40% prestressed beam the predicted maximum deflection, (Eq. 2), and ultimate load were determined to be 20 mm and 90 kN, respectively. For the non-prestressed beam the predicted ultimate deflection, (Eq. 3), and the ultimate load were estimated to be 46 mm and 90 kN.

The predicted maximum deflection at the mid span using moment curvature approach for the non-prestressed and prestressed beams was calculated to be 58 mm and 35 mm, respectively.

4.5.2 Deflection at cracking load

For non-prestressed beam, the predicted defection using (Eq.3) at the mid span was determined to be 0.4 mm at cracking and the associated cracking load was 20 kN. For the prestressed beam, the predicted deflection using (Eq.2) at mid span was 1 mm at a cracking load of 45 kN. The predicted deflection at cracking load using moment curvature approach is shown in Table 4- 1. Predicted load-deflection curves using moment curvature are plotted as shown in Figure 4-8 for non-prestressed and prestressed beams.

***Table 4- 1** Predicted deflection*

			ACI	Moment Curvature
Prestressed Beam	Ultimate	Load (kN)	90	90
		Deflection (mm)	20	35
	Cracking	Load (kN)	45	45
		Deflection (mm)	1	0.8
Non-prestressed Beam	Ultimate	Load (kN)	90	90
		Deflection (mm)	46	58
	Cracking	Load (kN)	20	20
		Deflection (mm)	0.4	0.4

4.3 Non-Prestressed Beam

4.3.1 Mode of Failure

The first specimen tested under monotonic load was a non-prestressed beam which served as a control beam for the non-prestressed beams. Its load versus deflection curve is shown in Figure 4- 2. The concrete cracked at a load of 10 kN. However, the expected cracking load was 20 kN. The first hairline cracks appeared in the form of flexural cracks in the constant moment region. Four cracks occurred at the same time, two in the middle of the constant moment region and the other two just outside of the constant moment region. At this point, the slope of the load deflection curve decreased indicating that flexural stiffness of the beam had decreased.

As the load increased, more flexural cracks appeared in the two shear spans of the beam, as shown in Figure 4- 3. Then a longitudinal crack occurred on the bottom of the midspan of the beam at a load of 38 kN. The cracks in the constant moment region grew vertically as the load increased. When the load reached 85 kN, which was slightly lower than the expected ultimate

load 90 kN, the basalt rebar ruptured, as expected, followed immediately by crushing of the concrete at the top of the beam as shown in Figure 4- 4.

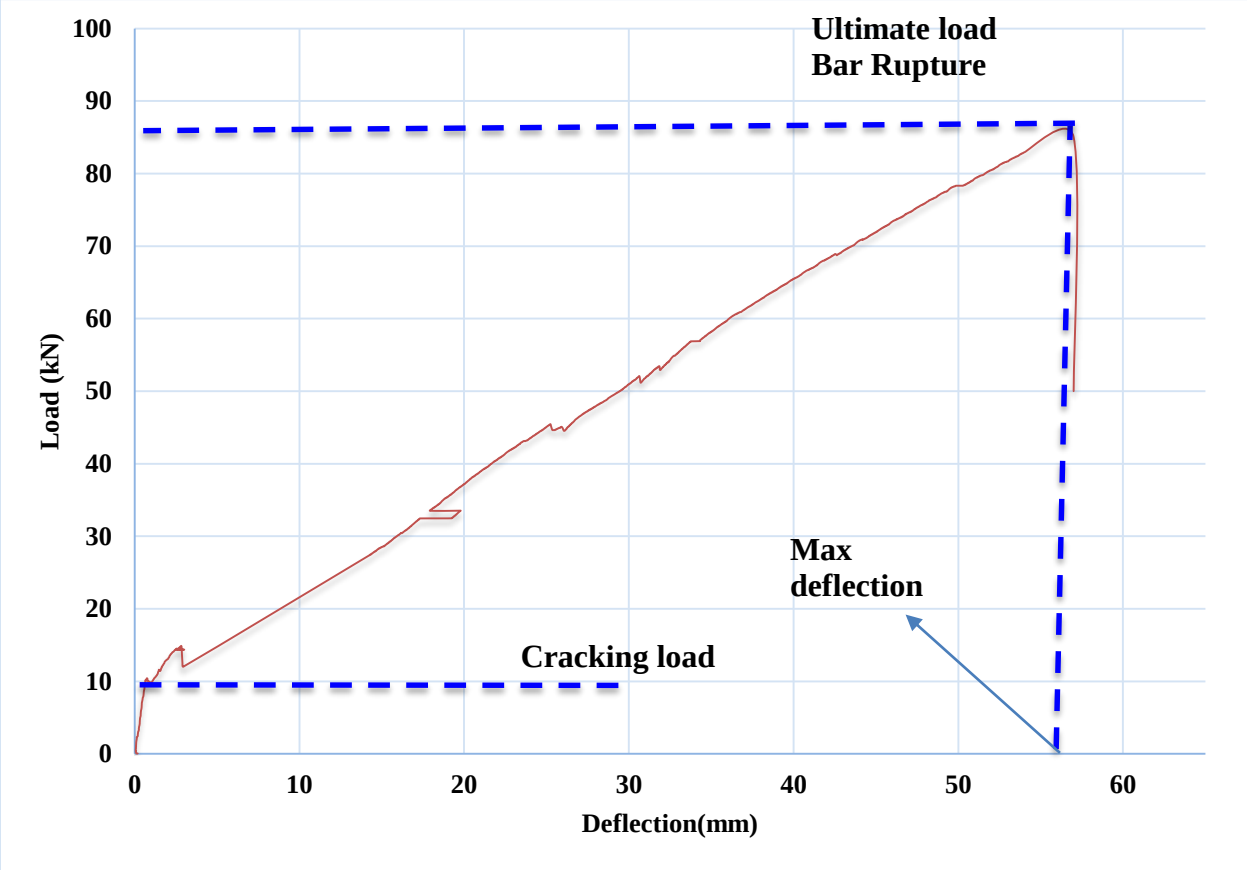

Figure 4- 2 *Load deflection curve for non-prestressed beam under static loading*

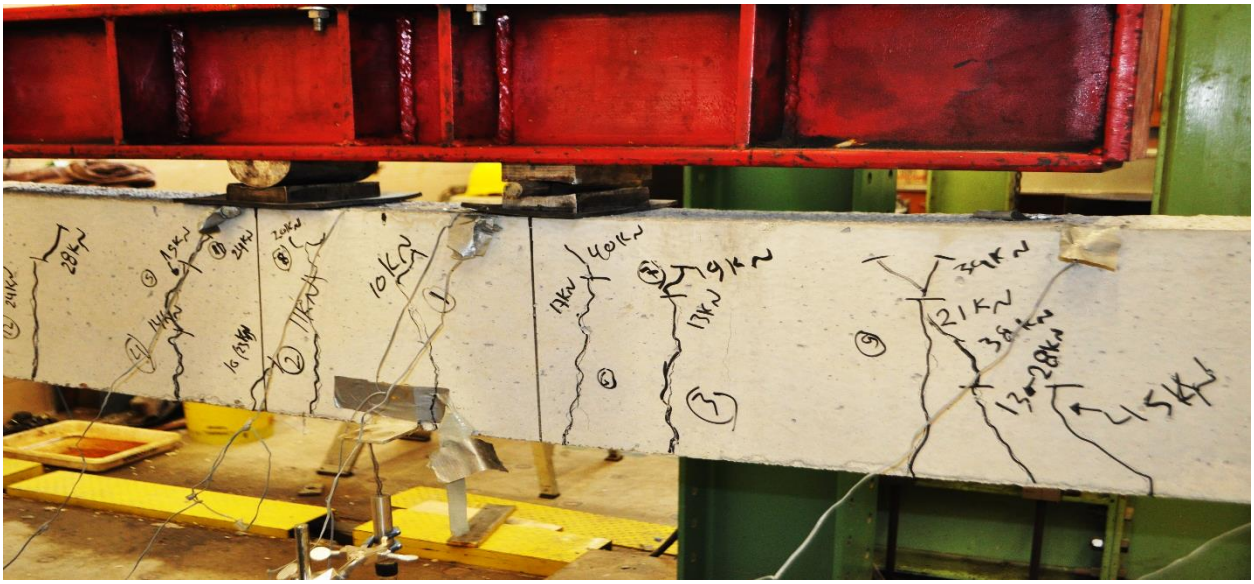

Figure 4- 3 *Cracks propagation inside and outside moment constant region (non-prestressed beam)*

Figure 4- 4 *Mode of faliure of a non-prestressed beam*

4.4 Prestressed Beam 40%

4.4.1 Mode of Failure

The same set up and loading conditions that were used in the previous beam were followed in testing this specimen**.** One BFRP beam prestressed to 40% of tensile bar strength was loaded monotonically to failure and served as a control for the prestressed beams. The load versus deflection curve for the test is shown in Figure 4- 5. It was expected that this beam would exhibit the same ultimate capacity as the non prestressed beam; however, the cracking load was expected to be higher. As in the previous beam, the first hairline flexural cracks appeared in the tension region of the beam started to form when the tensile stress in the concrete had exceeded its tensile strength at an applied load of 33 kN, which was lower than the expected cracking load 45 kN. Cracks were observed in the moment constant region and just outside of the constant moment region and the slope of the load-deflection curve decreased; as a result of the decreased flexural stiffness of the beam.

Then flexural- cracks occurred on both sides of the shear spans of the beam when the load reached 40 kN followed by a sudden formation of longitudinal cracks at the midspan on the bottom face of the beam. At 45 kN all of the strain gauges failed.

The cracks outside of and in the moment constant region grew vertically as the load increased. When the load reached 85 kN, a compression failure occurred with crushing of the concrete at the top of the beam, then the load dropped until bar rupture and complete collapse of the beam took place at a load of 65 kN as shown in Figure 4- 6. The expected bar rupture as a mode of failure did not occur. Reasons for the change to concrete crushing from the expected bar failure may be the close proximity of the provided reinforcement ratio to the balanced ratio,

(0.003165 and 0.003598, respectively). Also, the concrete compressive strength of 50 MPa after 28 days was less than the design value of 55 MPa.

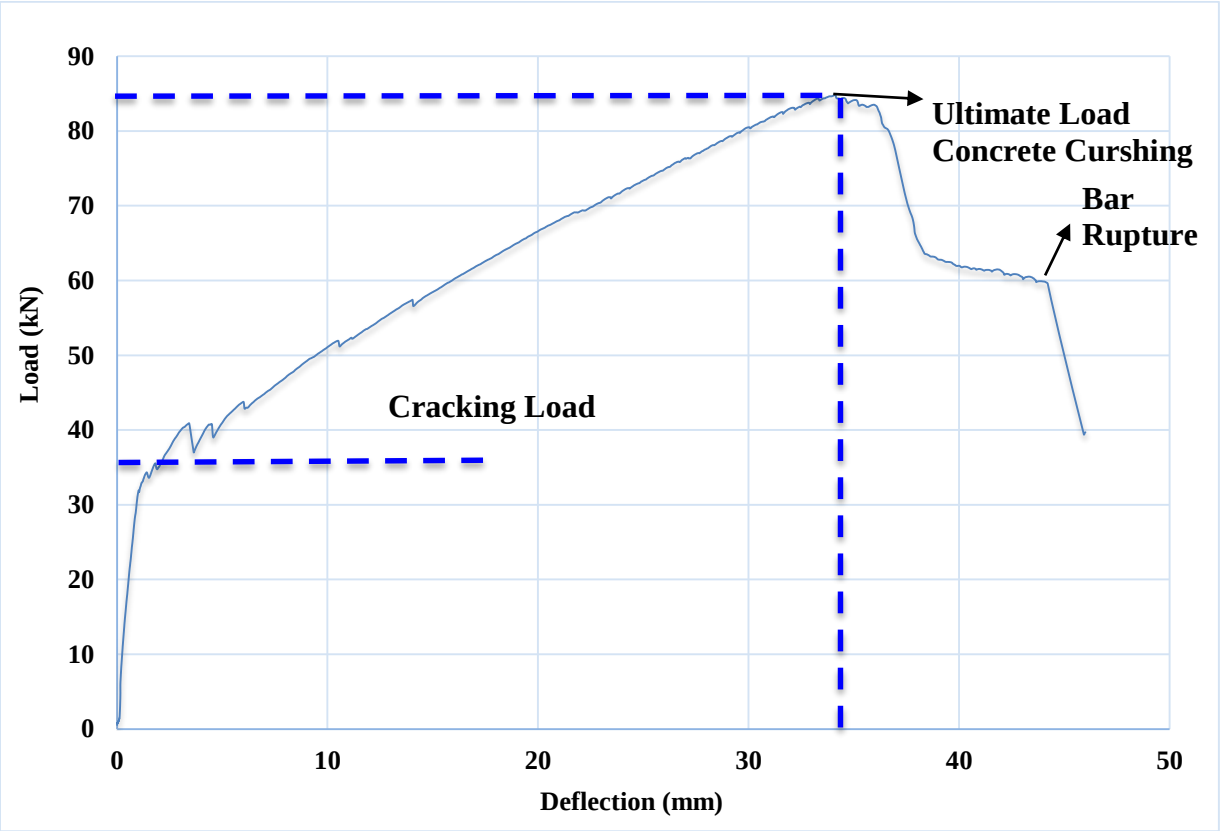

Figure 4- 5 *Load-deflection curve for 40% prestressed beam under static loading*

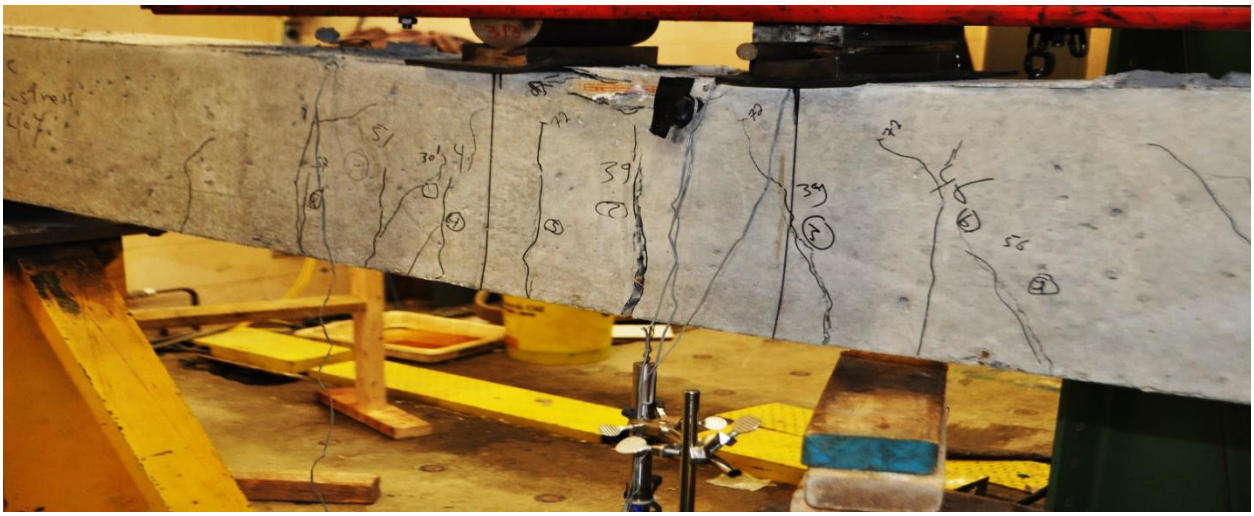

Figure 4- 6 *Mode of faliure of 40% prestressed beam under static loading*

4.5 Discussion of Deflection

The measured cracking load for the non- prestressed beam was 10 kN with a corresponding midspan deflection of 1 mm, and the cracking load for the prestressed beam was 33 kN with a corresponding mid span deflection of 4 mm. As expected the cracking load for the prestressed beam was higher than the non- prestressed beam. The maximum load was 85 kN for both the non-prestressed and prestressed beams with corresponding midspan deflections of 57 mm and 33 mm, respectively. As expected, the mid span deflection at failure for the non-prestressed beam was greater than for the prestressed beam.

This deflection predicted by moment curvature approach for the non-prestressed and prestressed beams was close to the experimental deflection 57 mm and, 33 mm for non-prestressed and prestressed beams, respectively. However, it was noticeably different from the 46 mm for the non- prestressed beam and 20 mm for the prestressed beam predicted by the relationships given by equations (2) and (3). At failure there was a rapid increase in deflection and large chunks of concrete fell off the beams. Figure 4-7 shows a direct comparison between the measured deflections for non-prestressed and prestressed beams.

Table 4- 2 summarizes the calculated and measured deflection at ultimate and cracking loads. Figure 4- 8 shows a direct comparison for measured and predicted deflection using moment curvature approach for non-prestressed and prestressed beams.

Table 4- 2 *Measured and predicted deflection*

			ACI	Moment Curvature	Experimental
Prestressed Beam	Ultimate	Load (kN)	90	90	85
		Deflection (mm)	20	35	33
	Cracking	Load (kN)	45	45	33
		Deflection (mm)	1	0.8	4
Non-prestressed Beam	Ultimate	Load (kN)	90	90	85
		Deflection (mm)	46	58	57
	Cracking	Load (kN)	20	20	10
		Deflection (mm)	0.4	0.4	1

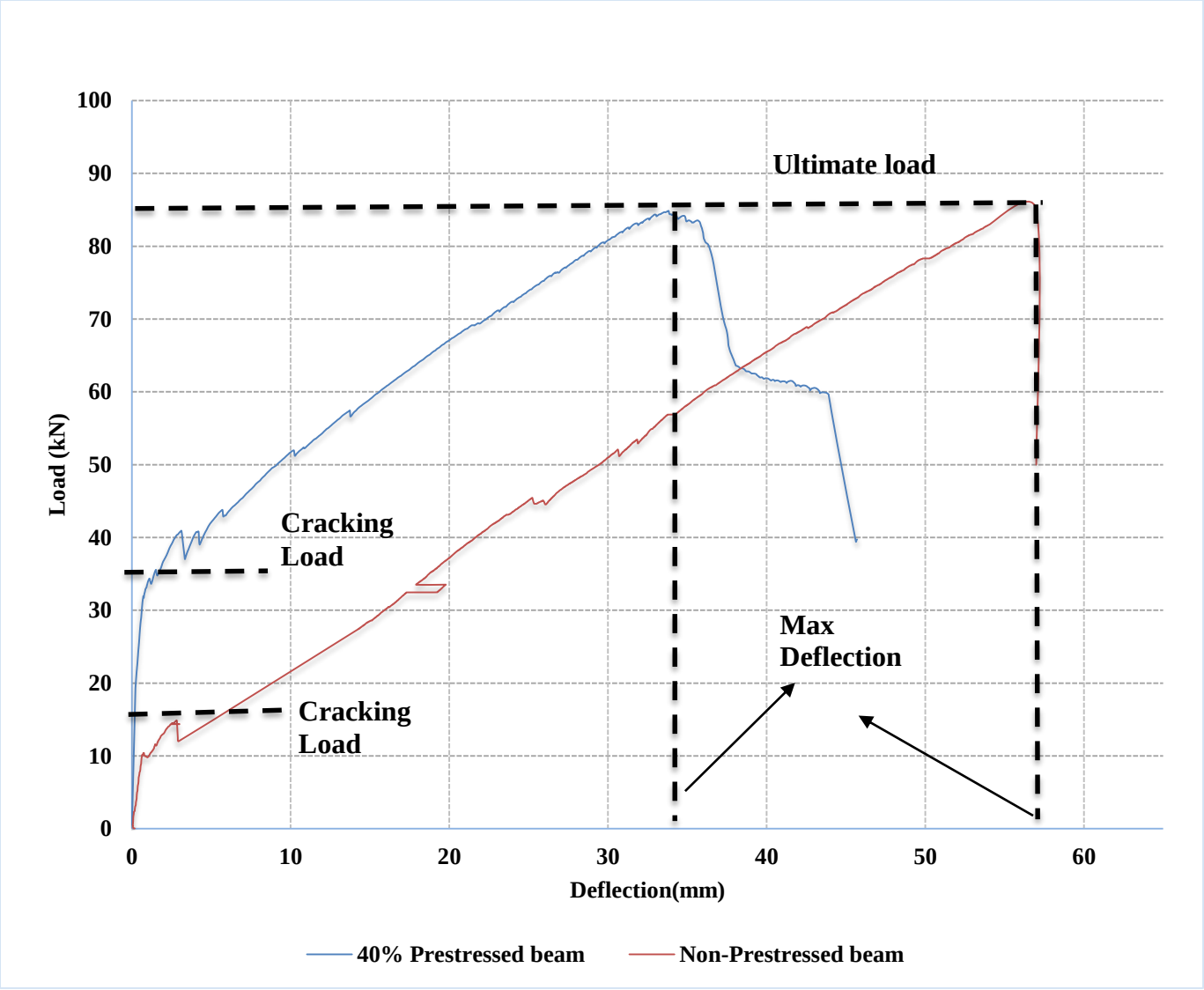

Figure 4- 7 *Measured load-deflection curves for non-prestressed and prestressed beams*

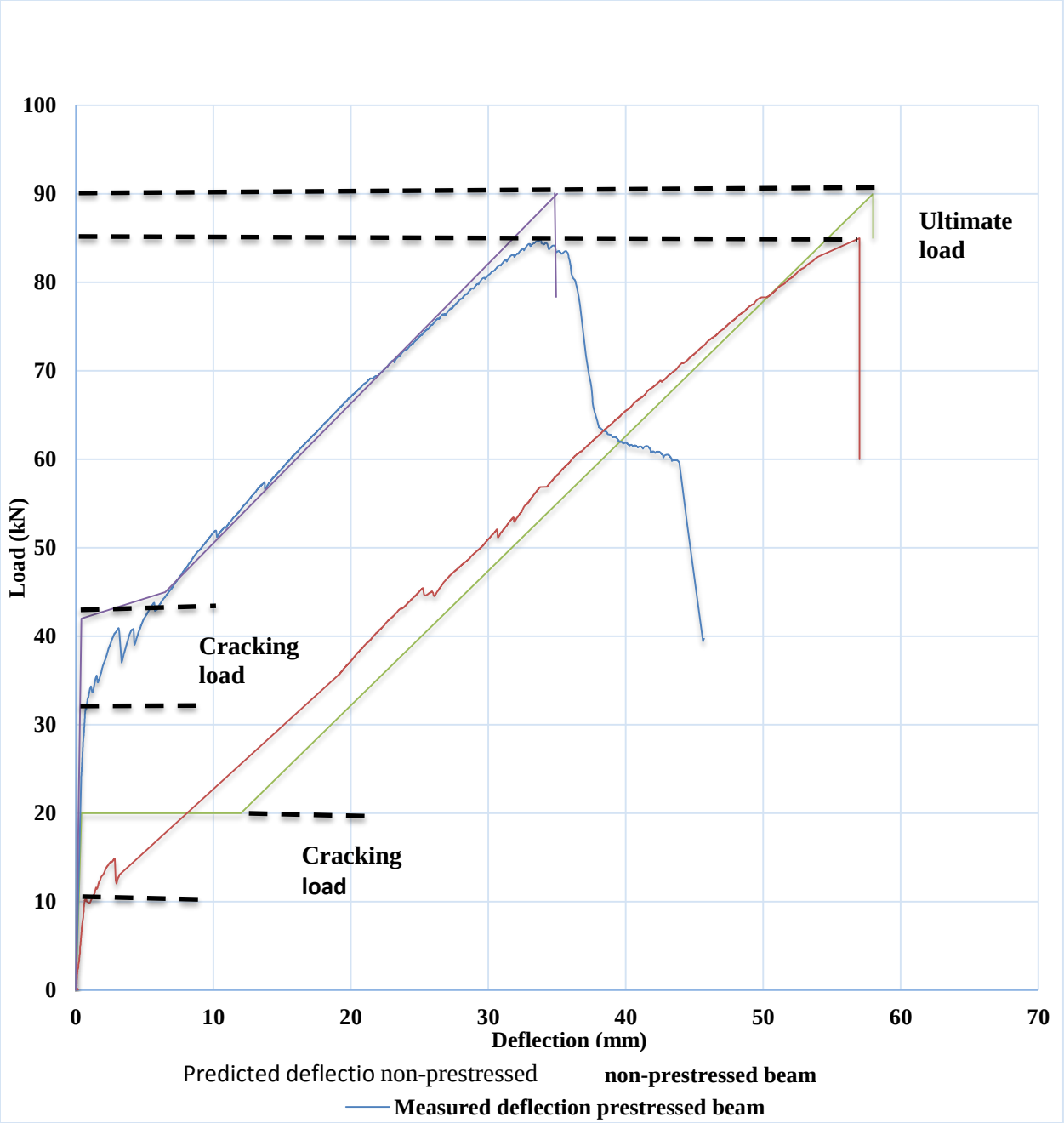

Figure 4- 8 *Predicted and measured load-deflection curves for non-prestressed and prestressed beams*

Chapter 5: Fatigue Test Results for Bare Basalt Bars

5.1 Introduction

This chapter presents the fatigue, creep and fatigue creep test results for the basalt bars tested in air. The mechanical and fatigue creep properties of the basalt bars are used together with an analysis of the beam stresses under the expected loading to calculate the minimum and maximum stresses and the stress ranges expected in the proposed beam fatigue tests. These predicted stress ranges are then used together with the basalt bar fatigue result to predict the fatigues lives of the proposed beam fatigue tests.

5.2 Fatigue Results of Bare Basalt Bars

Nine basalt bars were tested under fatigue loading. The stress ranges varied from 7% to 57.5% of the ultimate capacity of the basalt bars. The minimum stress in all the tests was kept constant at 40% of ultimate capacity of the bare bars approximately the same value as the calculated minimum stress in the proposed beam fatigue tests of beams.

The bar that was tested at a stress range of 7% of the ultimate capacity of bar failure load ran out to one million cycles. This bar was retested at a stress range simulating the stress range that would have been experienced by a beam tested at a stress range of 57.5 % of the control beam failure load. As shown in Figure 5- 1, the failure mode for these bars was by bar rupture in the region of reduced diameter of the bar. The bar fatigue data for both axes is plotted on logarithmic scales of stress versus fatigue life basis as in Figure 5- 2 and Table 5- 1 summarizes the fatigue lives for the bare basalt bar tests. In Figure 5.2 a dashed curve is shown in the high stress region where the extensive fatigue creep discussed in the next section led to failures at lives that fell below an extension of the linear log - log curve for fatigue failures.

Figure 5- 1 *Rupture of tested basalt bars under axial fatigue test*

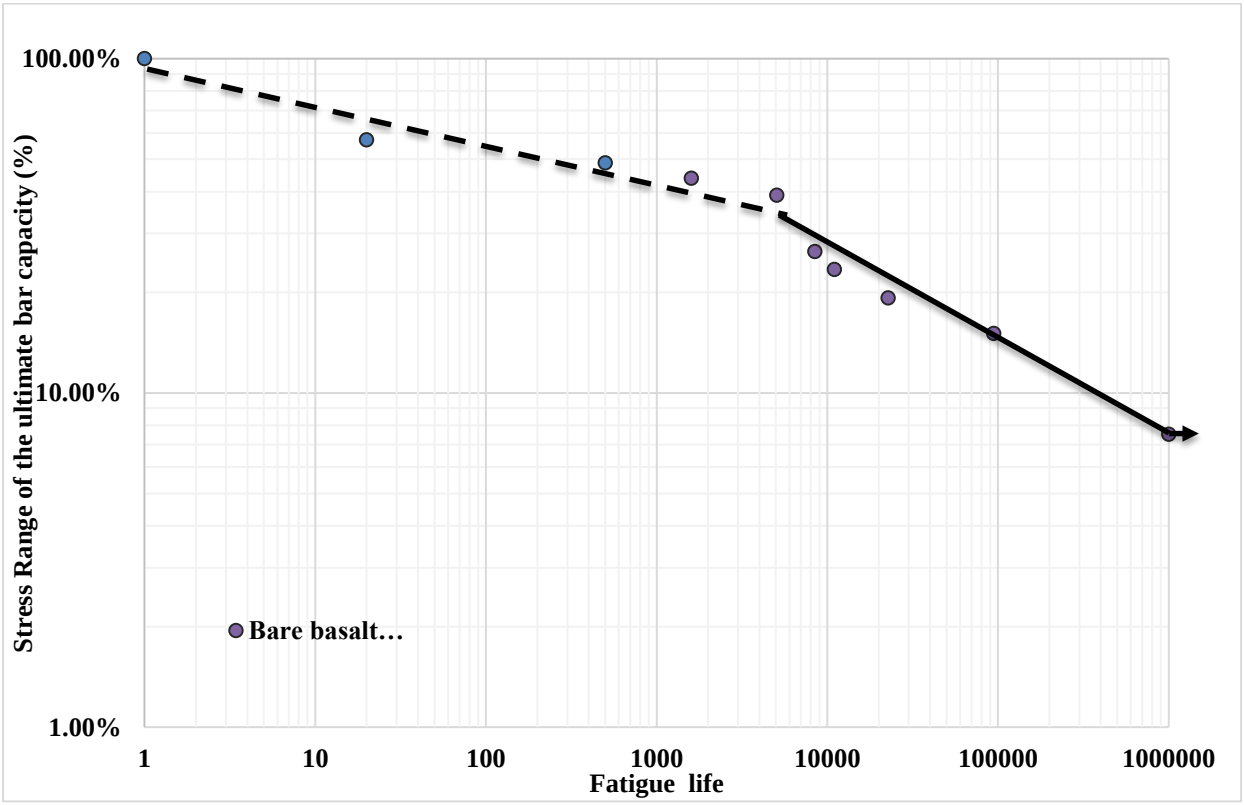

Figure 5- 2 *Fatigue life for bare basalt rebars*

Table 5- 1 *Fatigue life for bare basalt bars*

Notation*	Min Load (kN)	Max Load (kN)	Load Range	Fatigue life	Stress Range (%)
	------	36	36	1	100
FBB-1	14.5	35	20.5	20	57.50
FBB-2	14.5	32	17.5	500	48.7
FBB-3	14.5	30.25	15.75	1600	43.89
FBB-4	14.5	28.5	14	5047	39
FBB-5	14.5	24	9.5	8444	26.4
FBB-6	14.5	22.9	8.4	10977	23.4
FBB-7	14.5	21.4	6.9	22683	19
FBB-8	14.5	19.9	5.4	94323	15
FBB-9	14.5	17.2	2.7	1000000	7

* FBB: Stands for fatigue bare basalt bar, and the last number refers to the number of the specimen.

5.2.1 Creep and Fatigue Creep Behaviour

A typical curve of creep under sustained load is expected to show three different stages. There is an initial increase in elastic bar strain as the load is applied followed by a rapid increase in strain with time that slows to a period of steady state increase and finally at high stresses a rapid increase near failure for high stresses and for lower stresses a cessation of creep. The bare bar was tested under sustained load in order to investigate its creep behaviour.

Figure 5- 3 shows a plot of creep strain under sustained load versus time for a sustained load of 50% of the ultimate capacity of basalt bars. It is clear that the basalt bar did not experience creep strain at this stress level under sustained load.

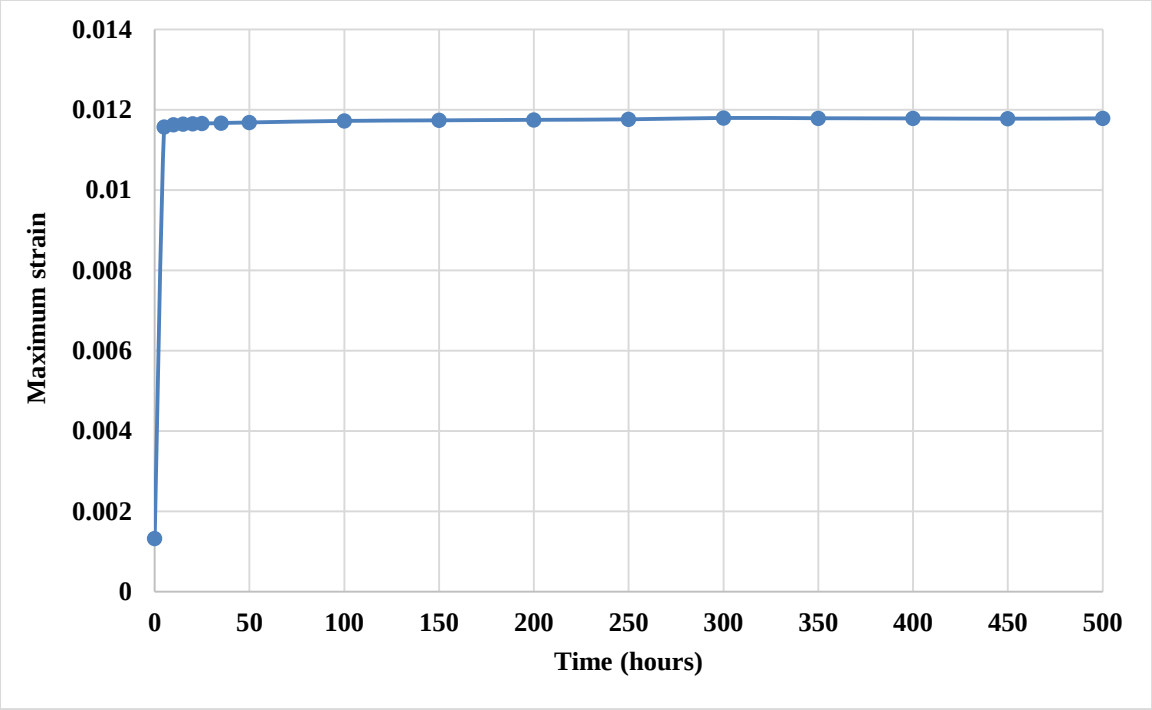

Figure 5- 3 *BFRP bar creep test*

The expected fatigue creep behaviour under fatigue loading is similar in form to creep under sustained load. Following an initial primarily elastic strain in the first cycle, the maximum strain in subsequent cycles increases first rapidly and then more slowly until near failure when it accelerates at high stresses. At lower stresses fatigue creep ceases. For the basalt bars cycled at stress ranges of 26.4%, 19% and 15% of the ultimate bar capacity, the second stage lasts most of the life as shown in Figure 5- 4. As the number of cycles increased, the strain increased nearly linearly until near failure. The steady state creep rate increases with increasing strain range. The strain gauges did not last until bar failure in the tests at the lower two stress ranges and the readings were terminated at 67% and 82% of the total number of cycles to failure in these specimens. Failure of the bars occurred by a progressive rupture of the fibers and their separation from the matrix.

Figure 5- 5 shows a relationship between the fatigue creep strain at one half of the fatigue life for tests with stress ranges of 26.4%, 19% and 15% of ultimate capacity of the basalt rebar. Another fatigue creep test performed on a bar without a reduced section tested at stress range equal to 19% of the ultimate stress of the machined bars produced fatigue creep results very close to those of the reduced section bars as shown in Figure 5- 4. The strain at half-life of the full bar was almost equal to that of the machined bar.

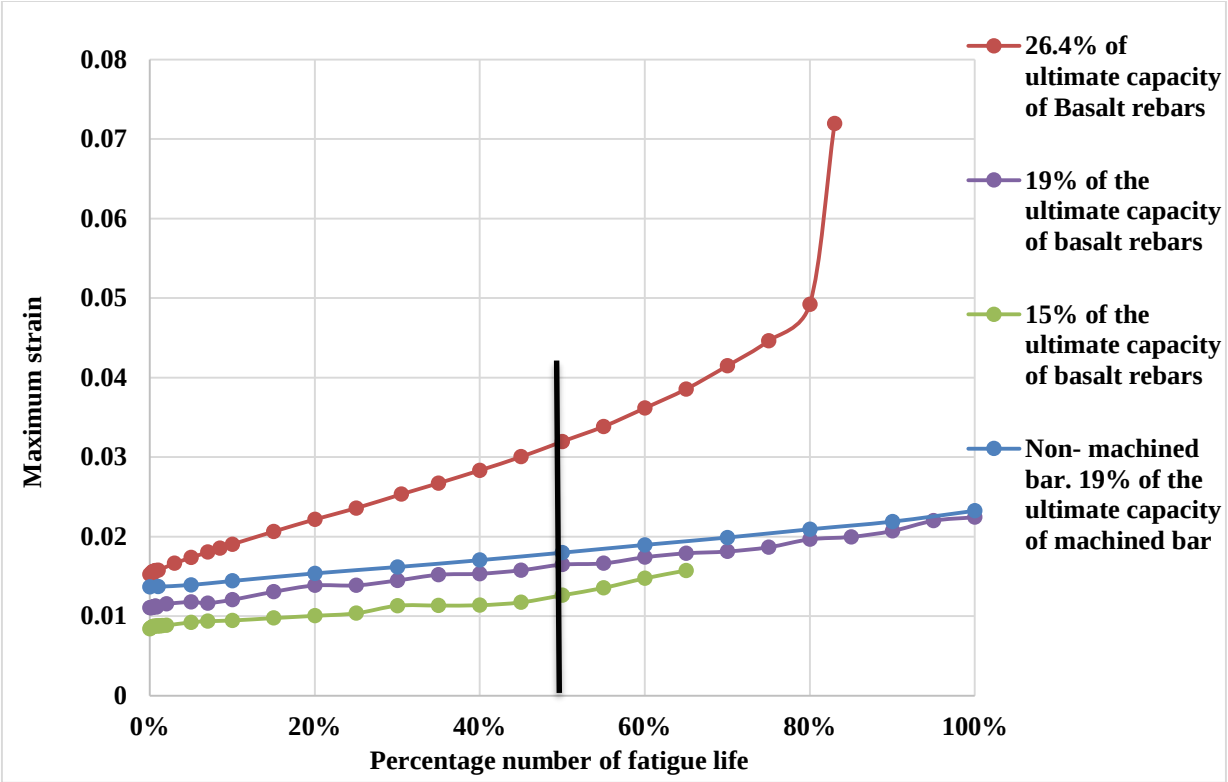

Figure 5- 4 *Machined and non-machined BFRP bar fatigue test – Fatigue creep strain with the percentage of fatigue life*

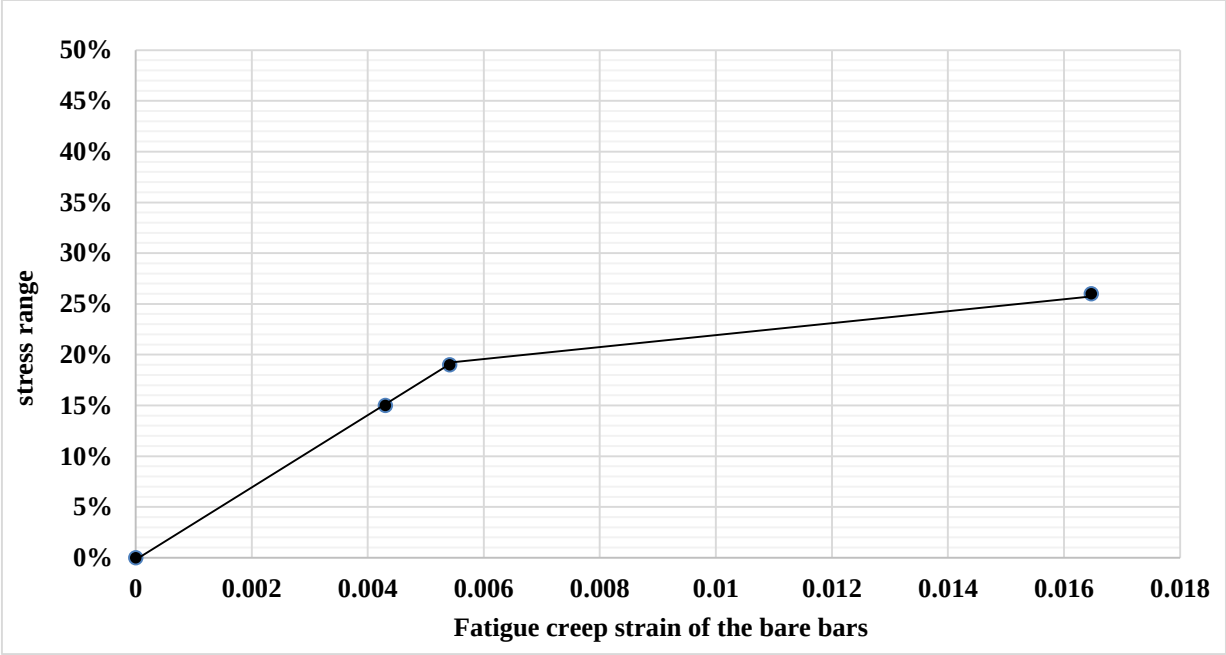

Figure 5- 5 *Fatigue creep strain of machined bare basalt bars at different stress ranges*

5.3 Prediction of the Fatigue Life for Non-Prestressed and Prestressed Beams

The predicted fatigue life for the non-prestressed and prestressed beams was calculated as follows:

1. A strain compatibility approach analysis was used to calculate the stress ranges in the beams for each of the proposed beam tests. The reductions in prestress level due to fatigue creep strain were then calculated from the half-life fatigue creep strain curve of Figure 5.5.
2. 2- The stress ranges that obtained from step 1 after taking into account the changes in stress range due to fatigue creep were entered in the stress range versus fatigue life curve of Figure 5.2 to obtain fatigue life predictions for the proposed beam tests and the expected fatigue lives are given in Table 5- 2.

Table 5- 2 *Fatigue test results for all beams*

Group	Description	Notation*	Load Range (%)**	Minimum stress (MPa)	Maximum stress (MPa)	Stress Range (%)	Expected Fatigue Life base on Bare Basalt Bars	Expected Failure mode***
One	Non-Prestressed Beams	F-0%-45	45	133	734	41	1000	BR
		F-0%-25	25	133	467	23	10000	BR
		F-0%-18	18	133	347	17	35000	BR
		F-0%-14	14	133	321	13	100000	BR
		F-0%-11.5	11.5	133	288	11	250000	BR
Two	40% Prestressed Beams	F-40%-80	80	133	1220	75	100	BR
		F-40%-60	60	133	900	53	300	BR
		F-40%-47.5	48	133	775	43	800	BR
		F-40%-35	35	133	635	34	2500	BR
		F-40%-27	27	293	590	20	20000	BR
		F-40%-20	20	435	573	9	300000	BR
Three	20% Prestressed Beams	F-20%-70	70	133	1377	65	190	BR
		F-20%-55	55	133	1080	51	500	BR
		F-20%-26	26	133	880	23	10000	BR
		F-20%-18	18	133	475	18	22000	BR
		F-20%-13	13	171	390	9	300000	BR

Notations:

* F stands for fatigue,0% non-prestress, 40% prestressing level, and 20% prestressing level, and the last number refers to load range.

. **Percentage of ultimate static load - *** BR: Basalt Bar Rupture.

Chapter 6: Fatigue Test Results for Non-Prestressed and Prestressed Beams

6.1 Concrete Beams

6.1.1 Non- Prestressed Beams Tested under Fatigue Loading

Five non-prestressed beams were tested under fatigue loading. The load range varied from 11.5% (9.78 kN) to 45% (38.25 kN) of the ultimate static capacity of the beam (85kN). The maximum load varied between 21.5% and 55% of the ultimate static capacity of the beam (between 18.27 kN and 46.75 kN). However, the minimum load was kept constant for all the beams and set to be 10% (8.5 kN) of the ultimate static capacity of the control beams. At the outset of the test, all of the beams were first loaded to the maximum load and then back to the mean load manually. While loading to the maximum load, flexural cracks were observed in and outside the constant moment region for all beams. During cycling, flexural cracks propagated and grew vertically and a longitudinal crack initiated on bottom face at the midspan of the beam.

The beam tested at 11.5% (9.78 kN) of the failure load of the control beam failed by bar rupture at 650,000 cycles. The extrapolated run out load range at one million cycles was 9% of the failure load of the control beam. The rest of the beams in this series were tested at load ranges equal to 45%, 25%, 18% and 14% of the control beam failure load. All of these beams failed by bar rupture in this series - none of the beams ran out. Figure 6- 1 shows the mode of failure for the beam cycled with load range of 18% of the control beam failure load.

Inspection of the broken bars and adjacent concrete pieces showed that the sand coating was missing from the bars and in some places still adhered to the concrete pieces as shown in Figure 6- 2. The bars showed surface scratches indicative of fretting between the sand or the

surrounding concrete and the bar as shown in Figure 6- 3. A similar failure mechanism has been reported by Katz (2000) and Noël (2014) who described extensive shearing of a sand coating and fretting of their GFRP bars.

Figure 6- 1 *Mode of failure of non-prestressed beam under fatigue load (load range 18%)*

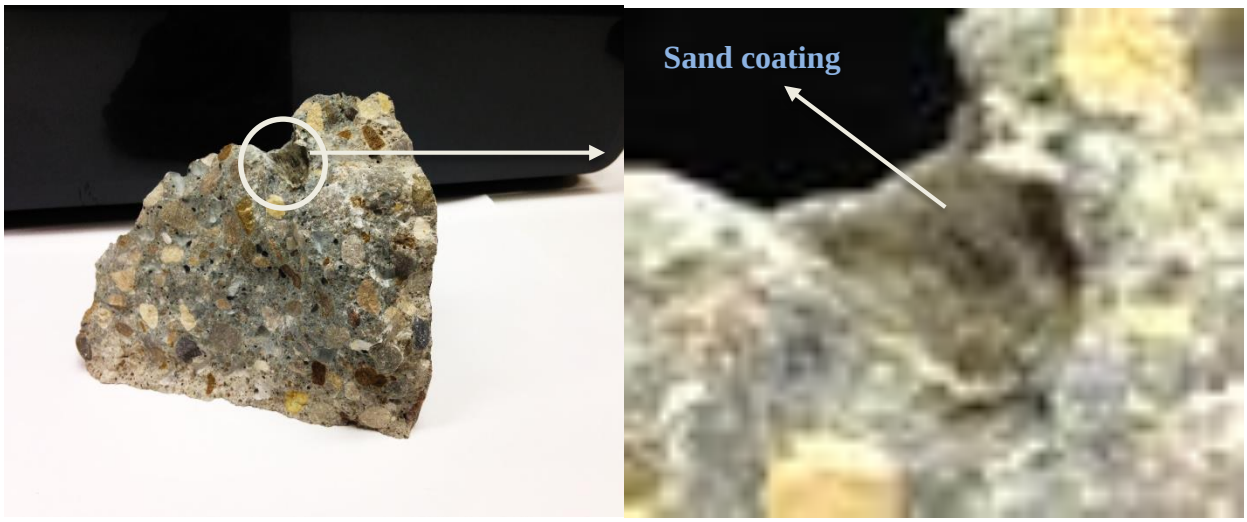

Figure 6- 2 *Adherence sand coating of basalt bars to the concrete surface*

Figure 6- 3 *Sand coating sheared off the basalt bars*

6.1.2 40 % Prestressed Beams Tested under Fatigue Loading

Five beams with their bars prestressed to 40% of their tensile strength were tested under fatigue loading. Before starting load cycling, all beams were first loaded to the maximum load in the load cycle and back to the mean load manually. During loading, flexural cracks appeared in and close to the constant moment region for all beams except for the beam that was tested at a load range of 20% (17kN) of the control beam failure load and ran out to one million cycles which had no cracks. While the beams were cycled, flexural cracks propagated and grew vertically and a longitudinal crack initiated on the bottom faces at the midspan of the beam. The beam tested at the lowest load range (20% of the control beam failure load) ran out to the one million cycle limit chosen and was retested at the highest fatigue load range of 80% of the control beam failure load where it failed after 184 cycles. In this test, the failure mode was a concrete crushing followed by bar rupture 14 cycles later. The expected mode of failure, bar rupture, did not occur possibly because extensive fatigue creep of the bar raised the neutral axis and led to increased concrete strains.

The other four beams were tested at load ranges of 60%, 47.5%, 35% and 27 % of the control beam failure load. All of these beams failed by bar rupture.

Similar to the previous specimens (non-prestressed beams) in this test series, an investigation of the broken bars showed that the sand coating was sheared off the bars and in some places was stuck firmly to the concrete pieces.

6.1.3 20% Prestressed Beams Tested under Fatigue Loading

Four beams with their bars prestressed to 20% of their tensile strength were tested under fatigue loading. As with the previous beams they were loaded to the maximum load and then unloaded to the mean load before fatigue loading began. During loading flexural cracks appeared in and close to the constant moment region for all beams except for the beam that was tested at a load range of 13% (11kN) of the control beam failure load and ran out to one million cycles which had no cracks. Again the minimum fatigue load was fixed for all the beams at 10 %(8.5kN) of the maximum capacity of the control beam. The test frequency for all tests was 3.5 Hz. The fatigue load ranges used were 70%, 55%, 26% 18% and 13%of the control beam failure load. The beam tested at a load range of 13% of the control beam failure load ran out to one million cycles and was retested at a load range of 70 % of the control beam failure load where it failed by concrete crushing. All of the other beams failed by bar rupture. As was observed for the previous beams, flexural cracks propagated and grew vertically and a longitudinal crack initiated on the bottom faces at the midspan of the beams during testing except for the beam tested at a load range 13% of the control beam failure load which did not exhibit any cracking. Also, as for the previous beam series, the bars of the failed beams showed scratching indicative of fretting.

6.2 Discussion

6.2.1 Fatigue Results

Table 6- 1 gives a summary of the fatigue lives of all the tested beams (non-prestressed, 40% prestressed and 20% prestressed) together with the expected fatigue lives calculated from bare basalt bar fatigue data in the previous section. The fatigue test results for the three sets of beams are plotted on logarithmic axes of load range versus cycles to failure as shown in Figure 6- 4 together with the predicted fatigue lives from Table 5.2 and 6.1.

Table 6- 1 *Fatigue test results for all beams*

Group	Description	Notation*	Load Range (%) **	Minimum stress (MPa)	Maximum stress (MPa)	Stress Range (%)	Expected Fatigue Life base on Bare Basalt Bars	Expected Failure mode	Actual Fatigue life (cycle)	Failure mode***
One	Non-Prestressed Beams	F-0%-45	45	133	734	41	1000	BR	3343	BR
		F-0%-25	25	133	467	23	10000	BR	19500	BR
		F-0%-18	18	133	347	17	35000	BR	64176	BR
		F-0%-14	14	133	321	13	100000	BR	242802	BR
		F-0%-11.5	11.5	133	288	11	250000	BR	650000	BR
Two	40% Prestressed Beams	F-40%-80	80	133	1240	76	100	BR	184	CC
		F-40%-60	60	133	970	57	300	BR	1,218	BR
		F-40%-47.5	48	133	800	46	800	BR	4,044	BR
		F-40%-35	35	133	635	34	2500	BR	8,363	BR
		F-40%-27	27	293	590	20	20000	BR	29,545	BR
		F-40%-20	20	435	573	9	300000	BR	1,000,000	Run Out
Three	20% Prestressed Beams	F-20%-70	70	133	1377	65	190	BR	146	CC
		F-20%-55	55	133	1080	51	500	BR	1,330	BR
		F-20%-26	26	133	880	23	10000	BR	20,574	BR
		F-20%-18	18	133	475	18	22000	BR	99,250	BR
		F-20%-13	13	171	390	9	300000	BR	1,000,000	Run Out

Notations:
* F stands for fatigue,0% non-prestress, 40% prestressing level, and 20% prestressing level, and the last number refers to load range.
. **Percentage of ultimate static load - *** CC: Concrete Crushing and BR: Basalt Bar Rupture.

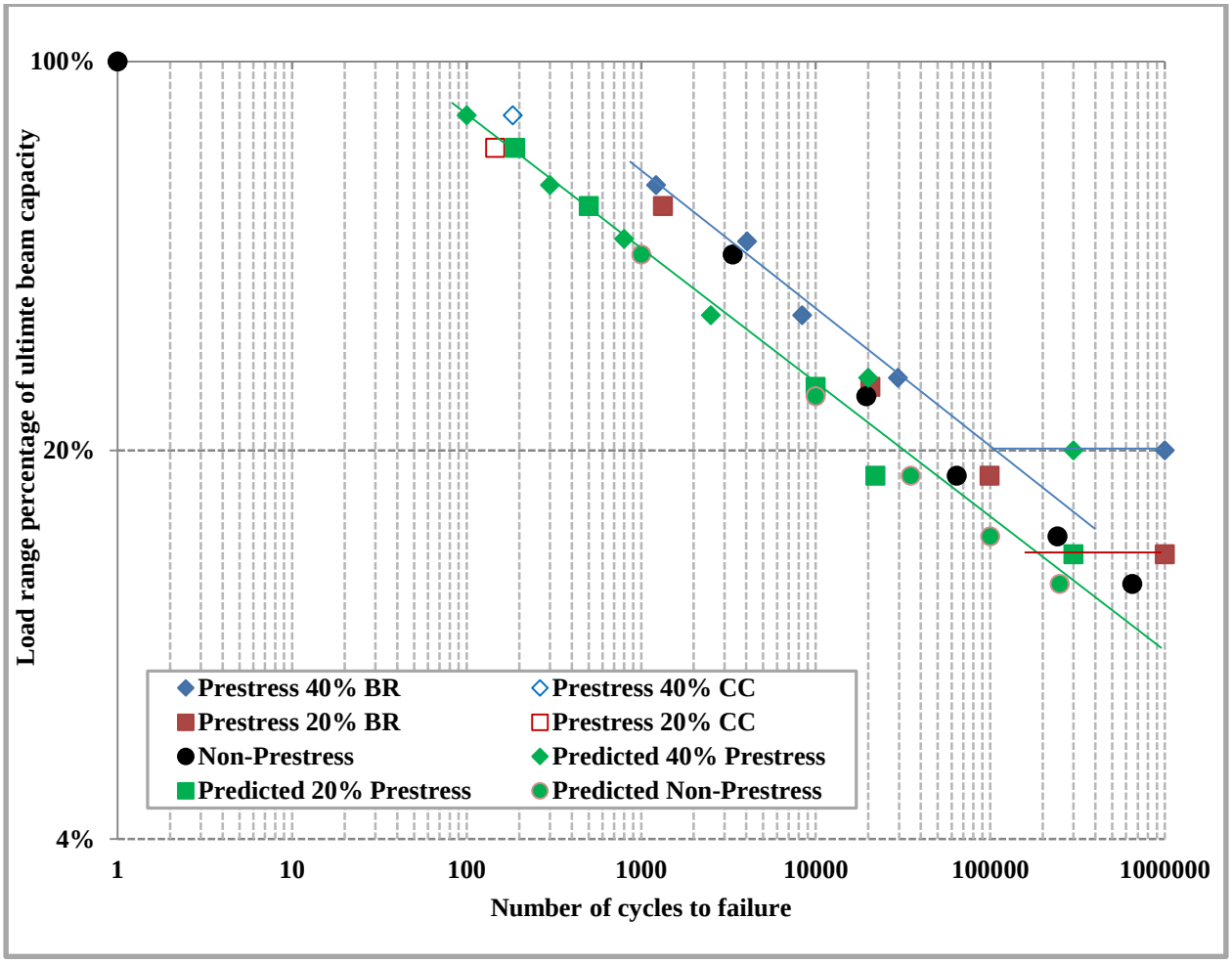

Figure 6- 4 *Measured and predicted fatigue life of non-prestressed, 40% and 20% prestressed beams*

The non-prestressed beam tested under monotonic load failed by bar rupture. Also, the beam prestressed to 40% of the ultimate capacity of the rebar tested under monotonic load failed by the concrete crushing (CC). Moreover, the 20% and 40% prestressed beams at the highest fatigue load levels failed by concrete crushing. For the rest of the cyclically loaded beams failure was by fatigue failure of the bars (BR).

Fatigue data for beams at the two levels of prestressed and for the non-prestressed beams fall into a compact band in the life region between 1000 and 100,000 cycles as shown in Figure

6- 4. This band is parallel to, but at fatigue lives more than twice, those predicted from the bare bar fatigue data. The discrepancy can be attributes to two factors. First an examination of the cross section of the bars indicated that the density of fibres was greater at the outside of the bars than in the reduced section of the machined bars used in the bar fatigue tests. This observation is consistent with the monotonic test results that showed that non-machined bars had a static strength 19 % greater than the machined bars. The second factor that may have reduced the fatigue strength of the machined bars below that of the non-machined bars in the beams was damage to the outer fibres during machining. The fatigue test results indicated that there was almost no benefit from prestressing in this life region. In the fatigue life region above 100,000 cycles, the predicted and observed fatigue strengths increased with the prestress level. The fatigue endurance limits, below which failure does not occur, fell close to the cracking loads of the beams. For the tests at shorter lives where prestressed and non prestressed beams fell on a single band, calculations of the prestress after fatigue creep indicated that the prestress decreased enough during cycling that the crack did not close at the minimum load and all beams were exposed to the same stress range at a given load range.

Beam fatigue data for the non- prestressed and two prestress levels is compared to the fatigue data for the machined bar specimens (not encased in concrete) as shown in Figure 6- 5. The bar fatigue data as expected show lower fatigue strengths at all fatigue lives than the beams. The curve drawn through the bar fatigue data falls parallel to the beam fatigue data at about one half the fatigue lives of the beams.

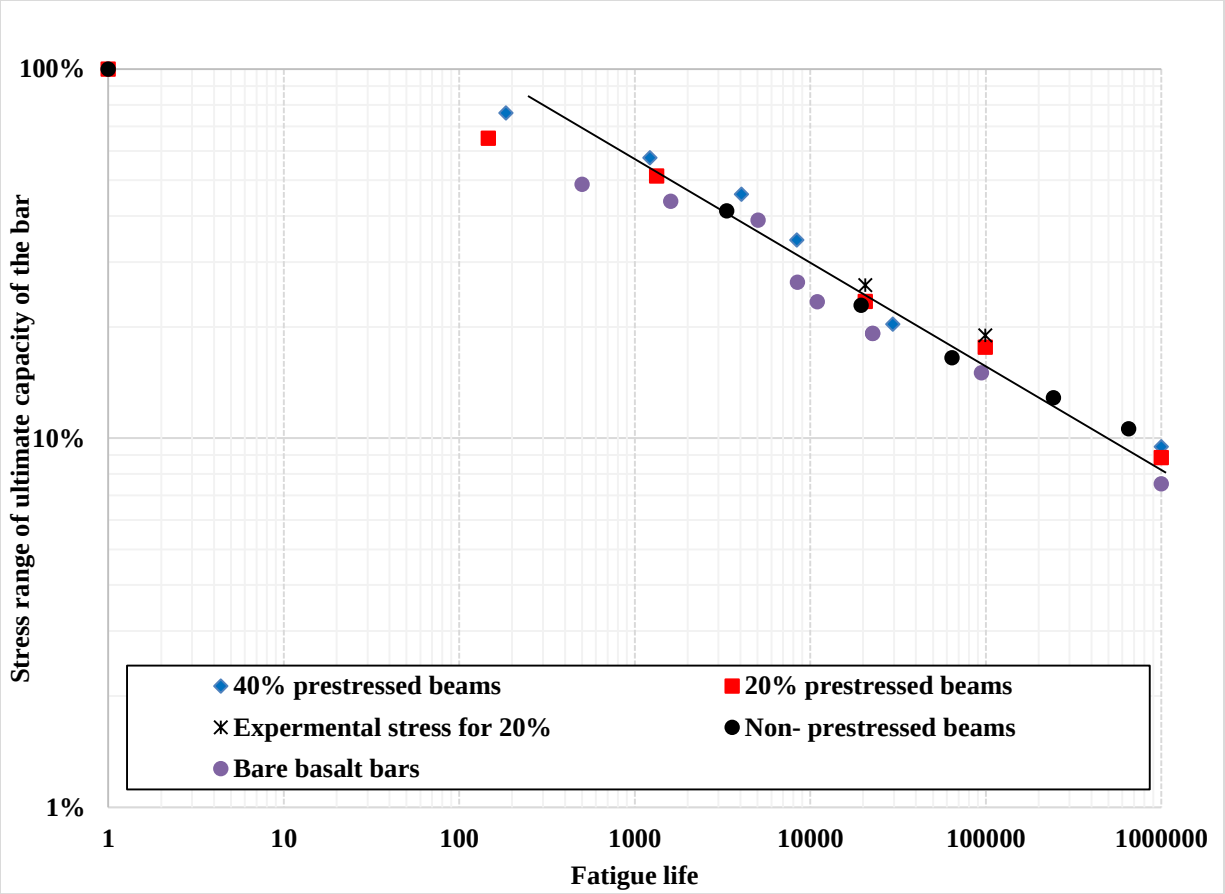

Figure 6- 5 *Fatigue Lives for bare basalt bars, non- prestressed and two levels (40% and 20%) beams*

The experimental setup lacked strain gauges capable of surviving the fatigue strains until the beams failed. Therefore no direct measurements of fatigue creep strains in the beam fatigue tests were obtained. This issue could be further investigated in future work, in which the experiments are done using additional suitable strain gauges in the experimental setup to measure the fatigue creep and provide a direct estimate of the loss of prestress.

6.2.2 Deflection Behaviour of Fatigue Loaded Beams

Figure 6- 6 shows typical curves of beam deflections over the fatigue life of the beams for two specimens prestressed to 20% of the bar rupture stress tested at load ranges of 55 and 70% of the failure load of the control beam respectively, two specimens prestressed to 40% of

the bar fracture stress tested at load ranges of 60 and 80% of the control beam failure load respectively and for two non-prestressed specimens tested at 45%and 25% of the control beam failure load, respectively. As was expected from the fatigue data, three stages are observed in the deflection behaviour of all of the beams tested under fatigue loading. In the first stage, the deflection increases rapidly for about 5% of the fatigue life of the specimens. In the second stage that lasted for about 90% of the fatigue life, there is a steady slow increase in deflection. In the final stage, the beams like the bars tested in cyclic creep showed a rapid increase in deflection.

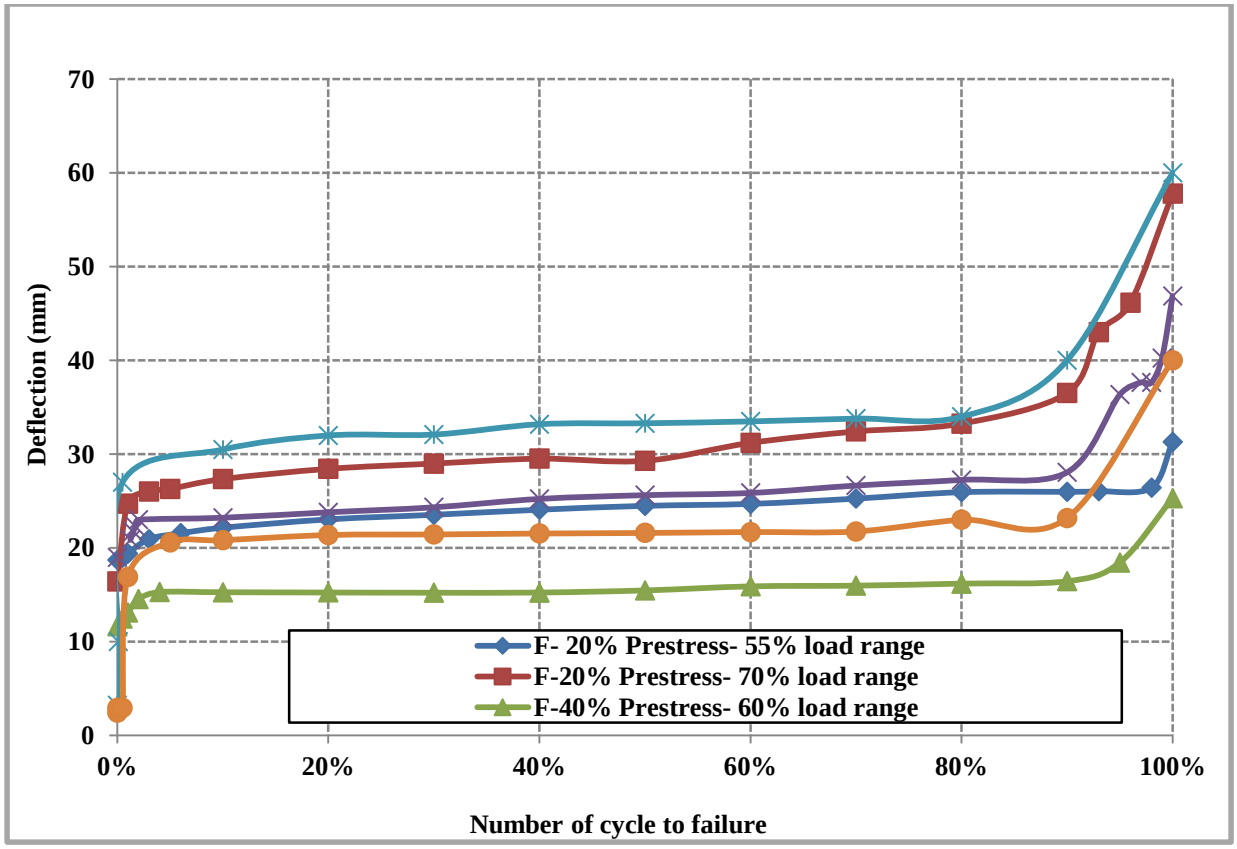

Figure 6- 6 *Deflection verses percentage number of cycles to failure*

Chapter 7: Conclusions and Recommendations

7.1 Conclusions

A total of 16 beams reinforced with non–prestressed and prestressed basalt bars were tested to failure. The first series consisted of six non-prestressed beams. The second series had six beams prestressed to 40% of the ultimate strength of the BFRP bar and the third series had four beams prestressed to 20% of the ultimate strength of the BFRP bar. All of the beams were tested under fatigue loading in load control except two beams, one from the first series and the other from the second series that were tested under monotonic loading in displacement control. In addition, thirteen machined bare basalt bars were tested to failure, three under monotonic loading, and nine in fatigue and one tested under sustained load.

A number of conclusions and recommendations were drawn from the experimental results:

1. For fatigue lives less than 100,000, cycles there was no improvement in fatigue strength due to prestressing. At the stress ranges in the bars in this life range, results of fatigue tests indicated that due to the loss of prestress due to creep crack closure due to the remaining prestress would fall below the minimum load in the test cycle. However, at fatigue lives above 100,000 cycles creep calculations indicated that enough prestress was retained to close the crack above the minimum load and prestress significantly increased the fatigue strength of both 20% and 40% prestressed beams.
2. The mode of failure of the prestressed beam reinforced with BFRP rebar tested under monotonic loading was due to the concrete crushing followed by bar rupture. This

unexpected result may be because the concrete compressive strength of 50MPa was lower than the target compressive strength of 55 MPa.

3. The mode of failure of the non- prestressed beam under monotonic loading was by bar rupture followed immediately by concrete crushing at the top of the beam.
4. The mode of failure of the prestressed RC beams reinforced with BFRP rebar tested under fatigue load at the highest load range for both levels of prestressing was by concrete crushing at the top; however, at all lower load ranges failure was by bar rupture.
5. The mode of failure of all the non- prestressed beams reinforced with basalt bars tested under fatigue load was by bar rupture as expected.
6. The monotonic loading deflections obtained for non-prestressed and prestressed beams were close to the deflections calculated theoretically by the moment curvature relationship. However, they were significantly different from those calculated using I_e as given by ACI 440.4R.
7. Load ranges of 20% and 13% of the monotonic loading strength of the basalt beams respectively are recommended as endurance limits for RC reinforced with 40% and 20% prestressed BFRP, respectively.
8. The fatigue limit at one million cycles of the bare BFRP bars was a stress range of 7% of their ultimate capacity.

7.2 Recommendations

1- Further fatigue creep tests would be useful to better define expected prestress losses due to this phenomenon on prestressing losses.

2- Strain gauges suitable for larger fatigue strains can be used to monitor bar strains throughout the bar fatigue life.

3- Concrete beams should be cast with one batch in order to get same compressive strength for all the beams. Using concrete with different batches might switch mode of failure.

4- Another study should be conducted in order to investigate the effect of prestress equal to 60% of the bar ultimate bar capacity on the fatigue limit of basalt bar reinforced beams.

5- Experimental study is needed in order to study fatigue life of full bare basalt bars.

6- More investigation is needed to study the distribution of the fibres over the cross section.

References

American Concrete Institute (ACI). (1997) "Considerations for Design of Concrete Structures Subjected to Fatigue Loading." *ACI 215-97*, Detroit.

American Concrete Institute (ACI). (2006) "Guide for the Design and Construction of Structural Concrete Reinforced with FRP Bars." *ACI 440.1R-06*, Detroit.

Alkhairi, F.M. (1991) "On the Behavior of Concrete Beams Prestressed with Unbonded Internal and External Tendons." *PhD Thesis, University of Michigan*, Ann Arbor, Michigan, p.415.

Al-Mayah, A., Soudki, K., and Plumtree, A. (2006) "Development and assessment of a new CFRP rod–anchor system for prestressed concrete." *Applied Composite Materials*, 13(5), 321-334.

Antrim J, C. (1967) "A study of the mechanism of fatigue in cement paste and plain Concrete." *Ph.D. Purdue University*, Purdue, 149 p.

Award, M.E., and Hilsdorf, H.K. (1974) "Strength and Deformation Characteristics of Plain Concrete Subjected to High Repeated and Sustained Loads." *ACI SP-41*, pp. 1-14.

Balazs, G. L. and Borosnyoi, A. (2001) "Long-term Behaviour of FRP." *Proceedings of the International Workshop Composities in Construction.* ASCE, Reston, pp. 84-91.

Braimah, A. (2000) "Long-Term and Fatigue Behaviour of Carbon Fiber Reinforced Polymer Prestressed Concrete Beams." *Ph.D. Thesis, Department of Civil Engineering*, Queen's University, Kingston, Ontario, 312 p.

Brik, V. (2003) "Advanced Goncept Goncrete Using Basalt Fiber/BF Gomposite Rebar Reinforcement." *Research and Technology Corp., Madison*.

Brondsted, P., Lilholt, H. and Anderson, S.I. (1997) "Fatigue Damage Prediction by Measurements of the Stiffness Degradation in Polymer Matrix Composites." *Proceedings of the International Conference on Fatigue of Composites Eight International Spring Meeting*, Paris, June 3-5

Burgoyne, C. J. (1993) "Should FRP Be Bonded To Concrete," *International Symposium on Fiber-Reinforced-Plastic Reinforcement for Concrete Structures*, Vancouver, Canada, Nanni, A. and Dolan, C. editors, American Concrete Institute, *ACI SP-138*, pp. 367-380

Chang, T.S. and Kesler, C.E. (1958) "Static and Fatigue Strength in Shear of Beams with Tensile Reinforcement." *Journal of the American Concrete Institute*, Vol. 29, No. 12: pp. 1033-1057.

Canadian Standard Associate (CSA). (2004) "Design of concrete structures." *CSA. A23. 3–04.* CSA, Rexdale, Ontario, 2004.

Curtis, P.T. (1989) "The Fatigue Behaviour of Fibrous Composite Materials." *Journal of Strain Analysis.* Vol. 24, No. 4: pp. 235-244.

Curtis, P. Fatigue. (1991) "Mechanisms in Unidirectional Polymer Matrix Composite Materials." *International Journal of Fatigue*, Vol. 13, No. 5: pp. 377-382.

Demers, C.E. (1998) "Fatigue Strength Degradation of E-glass FRP Composites and Carbon FRP Composites." *Construction and Building Materials*. Vol. 12, pp. 311-318.

Dorigato, A., and Pegoretti, A. (2012) "Fatigue resistance of basalt fibers-reinforced laminates." *Journal of Composite Materials*, 46(15), pp.1773-1785.

El-Ragaby, A., El-Salakawy, E. and Benmokrane, B. (2007) "Fatigue Life Evaluation of Concrete Bridge Deck Slabs Reinforced with Glass FRP Composite Bars." *Journal of Composites for Construction*, Vol. 11, pp. 258-268.

El Refai, A. (2013) "Durability and Fatigue of Basalt Fiber-Reinforced Polymer Bars Gripped with Steel Wedge Anchors." *Journal of Composites for Construction*, Vol. 17(6).

FIB. (2007) "FRP reinforcement in RC structures." Bulletin 40, *The International Federation for Structural Concrete FIB*, Lausanne, Switzerland

Glucklich, J. (1965) "Static and fatigue fractures of Portland cement mortar in flexure." *Proceedings of the First International Conferences on Fracture, 3*. The Japanese Society for Strength and Fracture of Materials, Sendai, Japan.

Heffernan, P.J. and Erki, M.A. (2004) "Fatigue Behaviour of Reinforced Concrete Beams Strengthened with Carbon Fiber reinforced Plastic Laminates." *Journal of Composites for Construction.* Vol. 8, No. 2: pp. 312-140

Holmen, J. O. (1982) "Fatigue of concrete by constant and variable amplitude loading." *ACI SP75*.

ISIS Canada 2008. Design Manual No.5-*Prestressing Concrete Structures with Fibre-Reinforced Polymers*, Winnipeg, Manitoba, Canada

Kato, T. and Hayashida, N. (1993) "Flexural Characteristics of Prestressed Concrete Beams with CFRP Tendons." *Fiber-Reinforced-Plastic Reinforcement for Concrete Structures, American Concrete Institute*, Vancouver, Canada, March 28-31, pp. 419-440.

Katz, A. (2000) "Bond to concrete of FRP rebars after cyclic loading." *Journal of composites for construction*, Vol.4, pp.137-144.

Kim, H.C. and Ebert, L.J. (1978) "Axial Fatigue Failure Sequence and Mechanisms in Unidirectional Fiberglas Composites." *Journal of Composite Materials*. Vol. 12: pp. 139-152.

Konur, O. And Matthews, F.L. (1989) "Effect of the Properties of the Constituents on the Fatigue." *Performance of Composites: A Review. Composites.* Vol. 20, No. 4: pp. 317-328.

Mindess, S., Young, J. F., and Darwin, D. (1981) "Concrete." *Prentice Hall*. Englewood Cliffs, Toronto, On.

Mohamed, N. (2013) "*Strength and Drift Capacity of GFRP-reinforced Concrete Shear Walls." PhD Thesis, University of Sherbrooke*, Sherbrooke, Quebec.

Murdock J., and Kessler C. E. (1960) "The mechanism of fatigue failure in concrete." *Report No. 587, University of Illinois, Illinois*.

Mutsuyoshi, H. and Machida, A. (1993) "Behaviour of Prestressed Concrete Beams Using FRP as External Cable." *International Symposium on Fiber-Reinforced-Plastic Reinforcement for Concrete Structures*, Vancouver, Canada, *American Concrete Institute*, ACI SP-138, pp. 401-417.

Noël, M., and Soudki, K. (2014) "Fatigue behavior of GFRP reinforcing bars in air and in concrete." *Journal of Composites for Construction*, Vol.18.

Pook, Les. (2007) "Why Metal Fatigue Matters." Solid Mechanics and Its Applications. *Springer Netherlands*, Vol.145, pp 161-165

Rafi, M., and Nadjai, A. (2008) "Experimental behaviour of carbon FRP reinforced concrete beams at ambient and elevated temperatures." *Journal of Advanced Concrete Technology*, pp.431-441.

Razaqpur, A. G., Svecova, D., and Cheung, M. S. (2000) "Rational method for calculating deflection of fiber-reinforced polymer reinforced beams." *ACI Structural Journal*, 97(1).

Reifsnider, K.L. (1991) "Damage and Damage Mechanics." *Fatigue of Composite Materials, Elsevier Science Publishing Company*, New York, United States, pp.11-78.

Rezansoff, T., Zacaruk, J.A., and Afseth, J.G. (1993). "High cycle (fatigue) resistance of reinforced concrete beams with lap splices." *Canadian Journal of Civil Engineering*, pp.642-649.

Saadatmanesh, H. and Tannous, F.E. (1999) "Relaxation, Creep, and Fatigue Behaviour of Carbon Fiber reinforced Plastic Tendons." *ACI Materials Journal*, Vol. 96, pp. 143-155.

Talreja, R. (1981) "Fatigue of Composite Materials: Damage Mechanisms and Fatigue-Life Diagrams." *Proceedings of the Royal Society of London*. Series A, *Mathematical and Physical Sciences*. Vol. 378, pp. 461-475.

Thompson, N. G., Yunovich, M., and Dunmire, D. (2007) "Cost of corrosion and corrosion maintenance strategies." *Corrosion Reviews*, pp.247-262.

Thun, H., Ohlsson, U., and Elfgren, L. (2007) "Tensile fatigue capacity of concrete." *Nordic Concrete Research*, Vol.36, pp.48-64.

Van de Velde, K., Kiekens, P., and Van Langenhove, L. (2003) "Basalt fibers as reinforcement for composites." *In Proceedings of 10th international conference on composites/nano engineering, University of New Orleans*, New Orleans, LA, USA (pp. 20-26).